Journal of Cosmology and Astroparticle Physics
An IOP and SISSA journal

Neutrinos from the cosmic noon: a probe of the cosmic star formation history

Riya[a] **and Vikram Rentala**[b]

[a]Department of Mechanical Engineering, Indian Institute of Technology Bombay, Powai, Mumbai 400076, India
[b]Department of Physics, Indian Institute of Technology Bombay, Powai, Mumbai 400076, India

E-mail: riyasingh@iitb.ac.in, rentala@phy.iitb.ac.in

Received August 1, 2020
Revised June 14, 2021
Accepted July 10, 2021
Published ???, 2021

Abstract. Multiple astrophysical probes of the cosmic star formation history (CSFH) indicate a period of peak star formation known as the cosmic noon between $1.5 \lesssim z \lesssim 3.5$. In this work, we explore the potential of future measurements of the diffuse supernova neutrino background (DSNB) at the Hyper-Kamiokande (HK) experiment to be sensitive to variations in the expected star formation rate at cosmic noon. Motivated by a statistically mild discrepancy between Hα and UV/IR probes of the CSFH, which indicate a factor of ~ 3 difference in the CSFH near the cosmic noon, we construct two benchmark hypotheses based on these different data sets. Since the cosmic noon neutrinos are redshifted to low energies, a low threshold sensitivity of any detector will be critical for discriminating between these benchmark hypotheses. We explore whether HK loaded with Gadolinium, with a positron threshold energy of 10 MeV, would be sensitive to the difference between these two CSFH hypotheses. Assuming that the supernova (SN) neutrino spectrum can be well determined by calibrating core-collapse SNe simulations to observations of nearby SNe, we find that only for very high core-collapse SN temperatures, HK would be sensitive to the difference in the benchmark CSFHs, and even then, over a 10–30 year time scale. Future experiments must lower their thresholds to be more sensitive to cosmic noon neutrinos.

Keywords: cosmological neutrinos, neutrino astronomy, star formation, supernova neutrinos

ArXiv ePrint: 2007.02951

https://doi.org/xxxxxxx

Contents

1 Introduction

Understanding the origin and evolution of galaxies is a problem at the frontier of cosmology. Observations of cosmic structure formation are generally in agreement with predictions of the ΛCDM cosmology indicated by other cosmological probes such as the cosmic microwave background (CMB) [1]. In particular observations of structure on large scales ($\gtrsim 10\,\mathrm{Mpc}$) appear to be consistent with purely gravitational dynamics, as seen in N-body simulations [2–4]. However, on smaller scales, the complex physics of galaxies and their evolution has a strong, and at the moment, incompletely understood, effect on cosmic structure. Several problems in small scale structure that appear to be in conflict with standard ΛCDM cosmology, such as the core-cusp problem [5–8] and the too-big-to-fail problem [9, 10], may possibly be resolved by a better understanding of the baryonic physics [11–14].

One of the critical ingredients to understand galaxy evolution is the cosmic star formation history. A variety of probes indicate a peak in the global (comoving) star formation rate density (SFRD) between redshifts $1.5 \lesssim z \lesssim 3.5$ [15], which suggests that this was the epoch of most vigorous star formation. This epoch is known as the *cosmic noon*. It has been estimated that nearly half of the stellar mass of the universe today was formed during this epoch.

A detailed prediction of the redshift and magnitude of the peak SFRD is lacking [16]. Qualitatively, it is expected that at early times the star formation rate grows as the dark matter potential wells grow and collect more gas, which in turn cools to form stars. At late times, the densities dilute due to Hubble expansion to the point where collisional cooling of the gas is inhibited, and new star formation in halos is suppressed. Thus, it is between these two extremes that one expects a peak in the global star formation rate [17]. However, complex feedback processes from galaxies such as stellar radiation, supernova explosions, and radiation from accreting massive black holes, lead to energy deposition in the interstellar medium (ISM) and circumgalactic medium, which would inhibit star formation, altering the cosmological peak in the SFRD history.

Moreover, there are a large range of galaxy masses (or length scales) that contribute to the cosmic SFRD, the effects of which can only be captured in large-volume cosmological simulations. Modelling the complicated effects of galactic feedback on the ISM in hydrodynamical, large-volume, cosmological simulations (for e.g. [18, 19]) is computationally unfeasible in the state-of-the-art simulations at the moment. Thus, simplified prescriptions for star formation efficiency and feedback mechanisms have to be invoked in these simulations using so-called sub-resolution parameters [4].

Turning this around, sub-resolution parameters are therefore *calibrated* by matching hydrodynamical simulations to observations. The SFRD history thus becomes one of the critical calibration observables for galaxy formation simulations [4]. Therefore, in order to understand galaxy formation and evolution, it is crucial to have a robust understanding of the CSFH from observations.

In this paper our objective is to explore the sensitivity of the Hyper Kamiokande neutrino experiment to the DSNB as a probe of the CSFH rate, especially to the cosmic noon neutrinos. We will first explore a comparison between inferences of the CSFH from UV/IR data and Hα data. We will show that the Hα data indicates a factor of ~ 3 larger peak in the SFRD at cosmic noon, as compared to the SFRD inferred from UV/IR data. Although this discrepancy is statistically mild, we use it to motivate the construction of two benchmark hypotheses for the CSFH. We will then describe how the Hyper-Kamiokande experiment will measure the spectrum of the DSNB and the limitations set on this measurement from various backgrounds. Finally, we will present our main results on the sensitivity of DSNB measurements at HK to the CSFH, and to the cosmic noon neutrinos in particular. We will do this by analyzing the ability of HK to distinguish between the two benchmark hypotheses. Throughout this paper, we use values of cosmological parameters taken from Planck [1]: $\Omega_m = 0.31$, $\Omega_\Lambda = 0.69$, and $H_0 = 67\,\mathrm{km\,s^{-1}\,Mpc^{-1}}$.

2 Probes of star formation history

A comprehensive review of different measurements of the SFRD inferred from various (electromagnetic) probes was made by Madau and Dickinson [15], here we will only attempt to summarize the main ideas.

In any standard inference of the star formation rate, mass is inferred from light in different wavelength bands. This conversion requires knowledge of the mass-to-light ratio, which depends on several factors such as galactic age, metallicity, star-formation history, extinction due to dust and initial (stellar) mass function (IMF). Currently, this ratio is obtained using stellar population synthesis models which compute the predicted spectral energy distribution (SED) of a galaxy with a given set of properties [20]. Synthesis models evaluate evolutionary tracks, i.e. how luminosity, temperature, and radius of stars vary as functions of mass and age and add in effects of stellar atmospheres to predict the spectra. The spectrum at a given galaxy age is then obtained by summing isochrone spectra of a population of stars over an assumed initial mass function.

UV and IR rest-frame emissions. The starlight from galaxies is typically dominated by young, bright, and massive stars which emit in the UV in the rest-frame of the galaxy. This UV light suffers extinction from the ISM and can be absorbed and re-emitted as mid- and far-infrared (MIR/FIR) light. Thus, two complementary strategies to study the SFRD are by measuring the rest-frame UV and IR emissions.

At low redshifts ($z \lesssim 1.4$), UV emission must be measured using space-based UV instruments. UV emission at larger cosmological distances is redshifted to optical bands, and thus deep surveys with ground based telescopes are a sensitive probe of this emission over a redshift range $1.4 \lesssim z \lesssim 6$. UV measurements are very sensitive to the assumed IMF, since the light is dominated by the emission from massive stars, but the total mass of the galaxy is dominated by low mass stars. Moreover, the age, dust extinction and metallicity of a galaxy can all lead to a reddening of the spectrum, making a prediction of the UV emission highly uncertain.

On the other hand, IR emission measurements with satellite based telescopes are sensitive to the SFRD over a lower range of redshifts ($z \lesssim 4$) than UV emission measurements. Inferring the SFRD from IR emission has the advantage of not being affected by further extinction due to dust, but the disadvantage is the complex emission process through which dust grains scatter light in the MIR/FIR range, which makes SED predictions very sensitive to the dust composition and emission models. Also, it is difficult to separate IR emission from star formation processes from IR emission from dust that has been warmed by older stellar populations or active galactic nuclei.

In Madau and Dickinson [15], luminosity functions at various redshifts were separately taken from several cosmological surveys that had measured rest-frame far-UV or mid- and far-infrared emissions. For each survey, these luminosity functions were then integrated to obtain co-moving luminosity densities, which were further multiplied by appropriate conversion factors, which were calibrated assuming a Salpeter IMF [21], to obtain the inferred SFRDs at a given redshift. The CSFH measured using UV data was then corrected for estimated dust attenuation based on the observed reddening of the rest-frame UV spectrum. The CSFH obtained from UV data after this dust correction was found to be in agreement with the CSFH obtained from IR data.

Madau and Dickinson [15] also provided a best-fitting function to the combined UV and IR data for the SFRD as a function of redshift as below:

$$R_{\rm SF}^{\rm UV/IR}(z) = 0.015 \frac{(1+z)^{2.7}}{1+\left[\frac{(1+z)}{2.9}\right]^{5.6}} \, M_\odot \, {\rm year}^{-1} \, {\rm Mpc}^{-3}. \tag{2.1}$$

Hα emission. UV radiation from massive ($M \gtrsim 17\, M_\odot$), young OB stars leads to photoionization and excitation of their surrounding gas nebulae. Recombination lines of hydrogen in H II regions, such as Hα and Lyα, can be used to measure the photoionization rate and hence probe the massive star formation rate. Among the nebular SFRD tracers, Hα lines in particular, are regarded as one of the most reliable and accessible tracers even in highly obscured star-forming galaxies (see for e.g. [22]). Wide-field, deep, narrow-band surveys are needed to use Hα as a probe of the CSFH. Currently, Hα probes have measured the CSFH out to a redshift of $z \lesssim 3$. Future observations with NASA's Nancy Grace Roman Space Telescope (formerly WFIRST-AFTA) [23, 24] and ESA's EUCLID mission [25] will give an even clearer picture of the Hα luminosity function at high redshifts and the inferred CSFH, especially around the cosmic noon [26]. The upcoming James Webb Space Telescope [27] will potentially enable the use of Hα SFRD measurements up to a redshift of 6 and possibly beyond.

A major limitation of using Hα emission as an SFRD probe is that extinction factors for Hα need to be modelled or calibrated by comparing Hα inferred SFRDs to FIR determined SFRDs or by using relative line strengths of O II and Hα (see for e.g. [28]). Additionally, active galactic nuclei (AGNs) can also cause ionization and thus lead to increased Hα emission. If

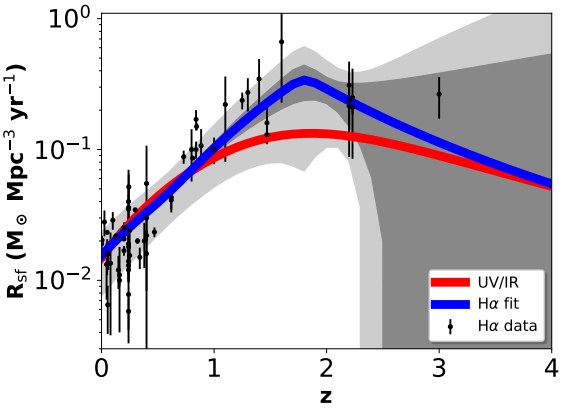

Figure 1. Cosmic star formation history: we show a comparison between the fit to the CSFH from UV/IR data eq. (2.1) (red curve) and our benchmark fit to the Hα data eq. (2.2) (blue curve) along with the 1- and 2-σ uncertainties (grey bands). The inferred SFRDs from Hα data with error bars (black data points) are also shown. At low-redshifts, the SFRD as inferred from Hα data is in agreement with the SFRD inferred from UV/IR data. However, there is a mild preference for a larger SFRD at cosmic noon indicated by the Hα data.

this contribution is not accounted for, the SFRDs inferred from Hα may be overestimated. We take the inferred SFRDs at multiple redshifts extracted from Hα data from [28–69] We have discussed our data selection and assumptions when correcting the original published data from these references in some detail in the appendix. We fit the CSFH from Hα data using a piecewise power-law parametrization similar to that of Horiuchi et al. [70]:

$$R_{\rm SF}^{\rm H\alpha}(z) = \dot{\rho}_0 \left[\left((1+z)^{\alpha\eta_1} + \left(\frac{1+z}{B} \right)^{\beta\eta_1} \right)^{\eta_2/\eta_1} + \left(\frac{1+z}{C} \right)^{\gamma\eta_2} \right]^{1/\eta_2}, \tag{2.2}$$

where $\dot{\rho}_0$ has dimensions of $M_\odot$ year^{-1} Mpc^{-3}. α, β, and γ are the power-law exponents in the low, mid, and high redshift regimes respectively and $|\eta_1|, |\eta_2| = 10$ are smoothing parameters. The constants B and C can be alternatively expressed in terms of constants z_1 and z_2 (which represent the transition redshifts between the low-mid and mid-high regimes) as, $B = (1+z_1)^{1-\alpha/\beta}$ and $C = (1+z_1)^{(\beta-\alpha)/\gamma}(1+z_2)^{1-\beta/\gamma}$. The signs of η_1 and η_2 in a generic fit should be chosen to agree with the signs of $\beta-\alpha$ and $\gamma-\beta$ respectively, in order to correctly interpret the parameters α, β, and γ as power-law indices in the appropriate redshift ranges.[1]

We fix the transition redshifts $z_1 = 0.6$ and $z_2 = 1.8$ and fit for the normalization and power-law indices using a chi-squared minimization technique. We find the following best-fit values: $\dot{\rho}_0 = 0.015$, $\alpha = 2.23$, $\beta = 3.78$, $\gamma = -3.27$. We have not considered the redshift errors on the Hα data when performing our fit.

The final inferred CSFH from Hα data and our best-fit function with the form of eq. (2.2) is shown in figure 1. We have also shown the uncertainty on the fit from a 1- and 2-σ variation of the fit parameters accounting for their correlations. Our fit is to be compared against the CSFH of Madau and Dickinson [15] in eq. (2.1) using UV/IR emission data which is also plotted in the same figure.

[1]Ref. [70] does not include the smoothing parameter η_1, which distorts the interpretation of the fitting function away from that of piecewise power-laws.

At low redshifts, the best fit Hα data and UV/IR data indicate similar CSFHs. Both the Hα and UV/IR data indicate a peak in the CSFH around $z \sim 1.8$, i.e. the cosmic noon, however, our Hα fit indicates a higher peak SFRD by a factor of ~ 3. This discrepancy is not statistically significant since the UV/IR CSFH lies within the 2-σ error band of the Hα CSFH fit.

We will however use the difference in the fits between UV/IR and Hα data to motivate two benchmarks CSFHs to test the sensitivity of Hyper Kamiokande to the CSFH and in particular to cosmic noon neutrinos. We will take the UV/IR CSFH of eq. (2.1) and our best-fit CSFH to Hα data parameterized by eq. (2.2) (both of which are shown in figure 1) as reference hypotheses for the CSFH. In the rest of this paper, we will explore the ability of future detection and measurement of the spectrum of the DSNB to resolve the difference between these CSFHs by ruling out one hypothesis in favor of another.

2.1 Note on other probes of the CSFH

Other probes to measure the CSFH include rest-frame radio emission from electrons in H II regions (see for e.g. [71]) and X-ray emission from newly formed X-ray binaries (see references in [15]). However, the radio emission signal is expected to be weaker from high redshifts where electrons lose energy due to scattering with the higher energy CMB photons at these redshifts. Moreover, calibration is difficult because of the unknown supernova and cosmic ray production rates which can inject free electrons into the gas, as well as the uncertain synchrotron efficiency. X-ray emission from AGNs dominates the cosmic X-ray background making X-ray observations also a less reliable tool to study the CSFH.

Another possible probe of the CSFH is to use the observed rate of core-collapse supernova (CC SNe) [72, 73]. This assumes that massive star formation and death is an approximately equilibrium process.[2] Unfortunately, poor statistics and dust-obscuration make the observed rate of CC SNe using emitted light unreliable as an SFRD indicator [74]. Another issue with using light to track the supernova rate is that many collapses may be intrinsically optically dark or dim [74, 75].

However, 99% of the energy emission from a CC SNe is expected to be in the form of neutrinos. Neutrinos from CC SNe form the diffuse supernova neutrino background, which is detectable in terrestrial neutrino detectors [70]. Using weakly-interacting neutrinos as a probe of the CC SNe rate has the advantage that the detectors have full-sky coverage automatically and neutrinos do not suffer dust obscuration. The downside is that the detection efficiency of neutrinos is low, which makes a measurement of the DSNB and consequent inferences of the CSFH difficult.

3 DSNB as a probe of the CSFH

The diffuse supernova neutrino background is the flux of neutrinos and anti-neutrinos from all CC SNe in the causally-reachable universe. The DSNB has yet to be discovered, although efforts are underway already at the Super-Kamiokande (SK) detector in Japan [76], and its proposed successor Hyper-Kamiokande (HK) [77]. These detectors primarily search for electron anti-neutrinos ($\bar{\nu}_e$) in the DSNB by looking for Cherenkov light from positrons created through the inverse β-decay processes ($\bar{\nu}_e + p \to e^+ + n$). While a discovery of the DSNB may be possible at the upgraded Super-Kamiokande gadolinium (SK-Gd) detector [78, 79],

[2] One reason why this is a good approximation is that the lifetime of massive stars is about 10 million years, which is very short compared to cosmological timescales.

characterization of the full spectrum of the DSNB, which is needed for extraction of the CSFH, would need a larger volume detector such as HK.

The expected DSNB flux spectrum at Earth is given by [80],

$$\frac{d\Phi}{dE_\nu} = \int_0^\infty \phi_{\rm SN}[E_\nu(1+z)] R_{\rm SN}(z)(1+z) \left| c\frac{dt}{dz} \right| dz. \tag{3.1}$$

Here, $\frac{d\Phi}{dE_\nu}$ is the differential arrival flux of neutrinos with incident energy E_ν. The right-hand side of this equation relates the arrival flux to the emission spectrum $\phi_{\rm SN}$ of neutrinos from a single "cosmologically-averaged" CC SN (where the arriving neutrino had an energy $E_\nu(1+z)$ at the time of emission) and the supernova rate density $R_{\rm SN}$ (measured in number/Mpc^3/yr) at redshift z. The redshift-time conversion factor over the redshift range of interest is given as usual by,

$$\left| \frac{dt}{dz} \right| = \frac{1}{H_0(1+z)} \frac{1}{\sqrt{\Omega_m(1+z)^3 + \Omega_\Lambda}} \tag{3.2}$$

for a ΛCDM universe.

The supernova rate can then be related to the star formation rate density at a given redshift by the relation [80],

$$R_{\rm SN}(z) = \frac{\int_8^{100} dM \left(\frac{dN}{dM}\right)}{\int_{0.1}^{100} dM \left(M \frac{dN}{dM}\right)} R_{\rm SF}(z) = \frac{R_{\rm SF}(z)}{135 M_\odot}, \tag{3.3}$$

where $\frac{dN}{dM}$ is the IMF, and we have made the assumption that all stars above $8\,M_\odot$ will end as CC SNe. To be consistent with the extracted SFRD assumptions in the previous sections, we have assumed a Salpeter IMF with $dN/dM \propto M^{-2.35}$ and a minimum and maximum stellar mass of $0.1\,M_\odot$ and $100\,M_\odot$, respectively.

3.1 Supernova neutrino emission spectrum

At the moment, we have a very limited understanding of the precise neutrino spectra emitted from a CC SN, or the diversity of neutrino spectra that are possible from different CC SNe. The only observational probe that we have is from SN1987A in the Large Magellanic Cloud, with $\mathcal{O}(10)$ neutrinos each seen by the Kamiokande [81, 82], IMB [83, 84] and Baskan [85] detectors. While a CC SN in the Milky Way would generate several thousand neutrino-detection signals in modern detectors such as the 32 kton SK experiment [86] or DUNE [87], the rate for galactic SNe is very low ~ 2.5 per century [88].

It has been proposed in ref. [89] to measure the neutrinos from CC SNe in the nearby universe (within ~ 10 Mpc) with a Mton scale detector, as a faster method for calibrating the CC SNe spectrum. With future Mton scale detectors such as Hyper-Kamiokande [90], UNO [91], and MEMPHYS [92, 93], we would be able to see ~ 1 neutrino per supernova, but the SN rate in this enlarged neighbourhood would also be larger ~ 1/year. A more recent, innovative proposal to look for CC SNe in our galactic neighborhood using archaeological lead-based cryogenic detectors to detect coherent, elastic neutrino scattering was suggested in ref. [94].

A detector mass scale of $\sim$ 5–10 Megatons (Deep-TITAND [95], MICA [96]) would permit observations of mini-bursts of neutrinos from CC SNe in nearby galaxies on a roughly yearly basis [97]. For a run of a few decades of such a 5 Mton detector, it is quite probable

that an SN occurs in one of the Milky Way, M31, M33, or their smaller satellite galaxies. This would lead to at least one burst with $\sim 10^2$–10^6 events.

These observations would feed in to calibration of numerical models of CC SNe [89, 98–103], and over the time scale of a decade or two, they could help us predict with much more precision the parameters describing the CC SNe neutrino spectrum. One additional advantage of these measurements is that the data would be averaged over many supernovae, which is useful if the emission from different CC SNe is less uniform than expected.

In this work, we will assume that the spectrum of CC SNe will be well characterized by a combination of simulations and possible calibration to observations of nearby SNe neutrinos, and we will neglect any uncertainty in the spectrum. For the rest of this paper, we will assume that the cosmologically-averaged CC SNe $\bar{\nu}_e$ spectrum (the type of DSNB neutrinos which are being looked for at SK and HK) is a pinched spectrum of the form [104],

$$\phi_{\rm SN}(E_\nu) = \frac{1}{6}\frac{E_{\rm tot}}{\bar{E}}\left(\frac{E_\nu}{\bar{E}}\right)^\alpha \frac{e^{-(1+\alpha)E_\nu/\bar{E}}}{\Gamma(1+\alpha)\bar{E}/(1+\alpha)^\alpha}. \tag{3.4}$$

This spectrum represents the effective time-integrated emission from the neutrino burst of a CC SNe with free parameters $E_{\rm tot}$, $\bar{E}$ and α. $E_{\rm tot}$ is the total energy emitted in the CC SNe explosion and the factor of 6 assumes equal partitioning into all neutrino flavors and in particular to $\bar{\nu}_e$. $\bar{E}$ is the average energy of an emitted neutrino, α is a pinching parameter with $\alpha \simeq 2.3$ giving an approximate Fermi-Dirac spectrum with a temperature $T \simeq \bar{E}/3.15$. We will fix $\alpha = 3$ based on fits to numerical simulations of the CC SN neutrino spectrum [105]. We will also use the definition of the parameter $T \equiv \bar{E}/3.15$ instead of $\bar{E}$ to characterize the spectrum, even though the spectrum is not Fermi-Dirac. We assume that the properties of cosmologically-averaged CC SNe (and hence the parameters $E_{\rm tot}$, T, and α) are redshift independent.

For SN1987A, with the sparse data that was observed, spectral parameters $E_{\rm tot} = 3\times10^{53}$ erg and $T \simeq 5\,$MeV were found to be consistent with the observations [80]. Different choices of $E_{\rm tot}$ give rise to different normalizations of the total DSNB flux. An estimate for the range of $E_{\rm tot}$ values based on the range of uncertainty of binding energies of neutron star final states is between $2.4\times10^{53}\,$erg and $3.5\times10^{53}\,$erg [106]. For the rest of this paper, we take the benchmark value of $E_{\rm tot} = 3\times10^{53}\,$erg. We will, however, consider several different benchmark temperatures, since the choice of temperature will crucially determine the shape of the spectrum and relative contribution of neutrinos from cosmic noon at a particular neutrino arrival energy. We will consider the benchmark scenarios where $T = 4, 5, 6, 8\,$MeV and "mixed" benchmark scenarios where $T = 6\,$MeV for a majority of the CC SNe, but between 10%–30% of CC SNe emit neutrinos with a temperature of 8 MeV. The latter cases represent a situation where a fraction of the DSNB is sourced by failed CC SNe (where the stellar collapse ends in direct black hole (BH) formation[3]), which are expected to have a higher effective temperature [107–109].

These benchmark spectra can be compared to predictions of simulations of CC SNe. The 1-d simulation of [110] which used a flux limited diffusion approximation indicated that $\bar{E} = 15.3\,$MeV, which would correspond to $T \simeq 4.9\,$MeV. However, more recent simulations [111–114], which take into account neutrino-radiation-hydrodynamics, find slightly

[3]Observational constraints are consistent with the bulk of stars above $18M_\odot$ collapsing to form black holes [132]. Assuming a Salpeter IMF, as we have, this would imply consistency with 30% failed CC SN.

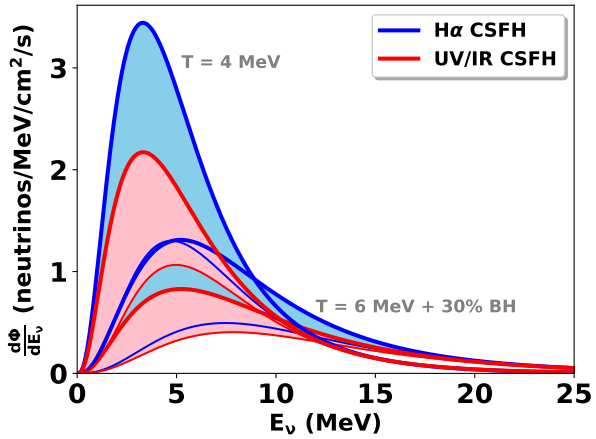

Figure 2. Predicted DSNB flux spectra assuming different CSFHs. The thick red curves show the flux spectrum assuming the UV/IR inferred CSFH and the thick blue curves show the flux spectrum assuming the Hα inferred CSFH. We have shown the spectra assuming two different temperature parameters $T = 4\,\mathrm{MeV}$ (curves with higher peaks) and $T = 6\,\mathrm{MeV}$ with a 30% BH component (curves with lower peaks, slightly shifted to the right). The shaded bands indicate the contribution to the DSNB flux from cosmic noon, i.e. from $1.5 \lesssim z \lesssim 3.5$. The rest of the flux is dominantly from redshifts $z \lesssim 1.5$. The difference in SFRDs at cosmic noon inferred from UV/IR data versus Hα data greatly accentuates the difference in the predicted DSNB spectra, especially at lower energies.

lower average energies of $\bar{E} = 10 - 14\,\mathrm{MeV}$ ($T = 3.2 - 4.4\,\mathrm{MeV}$). Thus, our lower benchmark temperature scenarios seem to be preferred by state-of-the-art CC SNe simulations. However, in this work we will adopt the view that calibration of the simulations to actual data is essential before establishing any definitive claims to an understanding of the spectral parameters of the CC SNe spectra.

The DSNB flux (eq. (3.1)) involves contributions of neutrinos from many different redshift slices, weighted by the SFRD at the corresponding redshift, where the spectrum from a given redshift slice is shifted in energy by a factor $(1+z)$. In figure 2, we show the predicted DSNB flux as a function of neutrino arrival energy for both the UV/IR CSFH from eq. (2.1) (thick red curves) and Hα CSFH from eq. (2.2) (thick blue curves) for the benchmark scenarios where $T = 4\,\mathrm{MeV}$ and $T = 6\,\mathrm{MeV}$ with a 30% BH component. Super-Kamiokande has set a DSNB flux limit of 3 neutrinos/cm^2/s above neutrino energies of 17.3 MeV [76]. For the $T = 8\,\mathrm{MeV}$ case, the integrated DSNB flux that we predict for the UV/IR (Hα) CSFH for neutrino energies $> 17.3\,\mathrm{MeV}$ is 1.5 (1.7) neutrinos/cm^2/s which is consistent with the limit set by SK. The location of the peak in the neutrino emission spectrum depends on the effective temperature. Since the neutrino spectra shifts towards lower energies at lower SN temperatures, all our other benchmark SN spectra hypotheses are consistent with the SK bound for either CSFH hypothesis.[4]

Since cosmological neutrinos are redshifted, the low energy DSNB is more sensitive to differences in the SFRD at the cosmic noon. We show the relative contribution of neutrinos

[4]In their 2003 analysis [133], SK had a threshold of 19.3 MeV for the neutrino energy and had set a flux exclusion limit of 1.2 neutrinos/cm^2/s above this energy. The 2003 limit was subsequently revised in a 2011 reanalysis [76] and the limit was weakened to 1.9 neutrinos/cm^2/s. We find a flux of 1.15 (1.24) neutrinos/cm^2/s above 19.3 MeV for the CC SNe temperature $T = 8\,\mathrm{MeV}$ for the UV/IR (Hα) CSFH. Both our CSFH hypotheses are thus consistent with this revised limit.

	Energy		Energy Range	
Temp	10 MeV	17.3 MeV	> 10 MeV	> 17.3 MeV
4 MeV	0.56 (0.66)	0.08 (0.08)	2.1 (2.3)	0.30 (0.29)
5 MeV	0.60 (0.78)	0.13 (0.13)	2.9 (3.3)	0.61 (0.60)
6 MeV	0.58 (0.81)	0.17 (0.18)	3.4 (4.1)	0.94 (0.96)
+10% BH	0.56 (0.80)	0.17 (0.19)	3.4 (4.2)	0.99 (1.0)
+20% BH	0.55 (0.79)	0.17 (0.20)	3.5 (4.2)	1.0 (1.1)
+30% BH	0.54 (0.78)	0.18 (0.20)	3.5 (4.3)	1.1 (1.2)
8 MeV	0.46 (0.70)	0.2 (0.25)	3.8 (5.0)	1.5 (1.7)

Table 1. Table of fluxes from the cosmic noon for given energies/energy ranges (columns) assuming the UV/IR CSFH. The rows correspond to different assumptions of the CC SNe temperature spectral parameter. Numbers in brackets indicate the corresponding fluxes assuming the Hα CSFH. The two columns on the left are fluxes at a specific energy and have units of neutrinos/MeV/cm^2/s, whereas the two columns on the right are fluxes integrated over the indicated energy range and have units of neutrinos/cm^2/s. The flux at lower threshold energies is significantly higher for the Hα CSFH, primarily due to the contribution of a larger fraction of neutrinos from the cosmic noon.

from the cosmic noon in figure 2, i.e. from redshifts $1.5 \lesssim z \lesssim 3.5$ using bands for the two CSFHs. The contribution from neutrinos beyond redshift 3.5 is negligible. From the figure, we can see that the contribution of neutrinos from the cosmic noon is significant at low neutrino energies. Moreover, it can be seen that the difference in the cosmic noon SFRDs inferred from UV/IR versus Hα data greatly accentuates the predicted difference in the neutrino spectra from these two CSFHs, especially at lower energies. For $T = 6$ MeV with a 30% BH component, the cosmic noon contributes 54% (64%) of the flux at 5 MeV and 13% (23%) at 15 MeV for the UV/IR (Hα) CSFH. At higher energies above 25 MeV, the cosmic noon contributes less than 10% of the DSNB flux.

The energy range of sensitivity to DSNB flux measurements at SK and HK are limited by various backgrounds which we will discuss in further detail in a later section. In order for DSNB spectral measurements to be sensitive to the differences in contributions from the cosmic noon for different CSFHs, it is advantageous to go to lower threshold energies. In their 2011 analysis setting an upper limit on the DSNB, SK had set a lower threshold of 17.3 MeV for neutrino energy which was limited by spallation backgrounds [76] and would not have been very sensitive to the cosmic noon neutrinos, even if the flux normalization was high enough to permit discovery of the DSNB. In the upgraded SK-Gd detector, it is expected that the threshold might be reduced to as low as ~ 10 MeV [79] and this could open up sensitivity to differences in neutrinos from the cosmic noon.

For the $T = 6$ MeV with 30% BH benchmark spectrum, we find an integrated flux of 3.5 (4.3) neutrinos/cm^2/s for neutrinos above 10 MeV for the UV/IR (Hα) CSFHs. Moreover, for the integrated flux in this range, 15% (25%) of the total neutrinos are from the cosmic noon.

In table 1, we give numerical values of the fluxes of neutrinos from the cosmic noon at various energies/energy ranges corresponding to different assumptions of the CC SNe temperature parameter for both the UV/IR and Hα CSFHs. In table 2, we show the relative fraction of neutrinos from the cosmic noon at these energies/energy ranges for different assumptions of the CC SNe temperature parameter. We can clearly see from these tables that measurements of the neutrino flux at lower threshold energies will be more sensitive to the cosmic-noon neutrinos.

	Energy		Energy Range	
Temp	10 MeV	17.3 MeV	> 10 MeV	> 17.3 MeV
4 MeV	0.10 (0.18)	$< 1\%$	0.04 (0.08)	$< 1\%$
5 MeV	0.18 (0.3)	0.02 (0.05)	0.08 (0.15)	0.01 (0.02)
6 MeV	0.27 (0.39)	0.06 (0.11)	0.12 (0.22)	0.02 (0.05)
+10% BH	0.28 (0.41)	0.07 (0.13)	0.13 (0.23)	0.03 (0.06)
+20% BH	0.29 (0.42)	0.08 (0.15)	0.14 (0.24)	0.04 (0.07)
+30% BH	0.30 (0.43)	0.09 (0.16)	0.15 (0.25)	0.04 (0.08)
8 MeV	0.40 (0.52)	0.15 (0.25)	0.20 (0.31)	0.07 (0.13)

Table 2. Table of DSNB flux fractions arising from the cosmic noon ($1.5 \lesssim z \lesssim 3.5$) assuming the UV/IR CSFH for given energies/energy ranges (columns). The rows correspond to different assumptions of the CC SNe temperature spectral parameter. Numbers in brackets indicate the corresponding fractions for the Hα CSFH. Measurements of the DSNB flux with a lower threshold will receive greater contributions from the cosmic noon and will thus be more sensitive to the differences between the UV/IR and Hα CSFH.

Next, we will discuss the proposed Hyper-Kamiokande experiment and explore whether HK would be sensitive to the difference in predicted neutrino fluxes under the two different hypotheses of UV/IR and Hα inferred CSFHs.

4 DSNB detection at Hyper-Kamiokande

Hyper-Kamiokande is a next-generation underground water Cherenkov neutrino detector, based on the Super-Kamiokande experiment [77]. Electron anti-neutrinos $\bar{\nu}_e$ are detected by looking for Cherenkov light from positrons created through inverse β-decay processes ($\bar{\nu}_e + p \rightarrow e^+ + n$), where the protons taking part in the inverse β-decay process are from hydrogen atoms in the water. The proposal for the HK experiment is to build two identical water Cherenkov detectors, each having a fiducial volume of 187 ktons. The first detector will be built in the Tochibora mine in Japan, and the second detector is proposed to be built in Korea [115].

The positron rate spectrum at HK is related to the incident neutrino flux Φ as [80, 116],

$$\frac{dN}{dE_{e^+}dt} = \frac{d\Phi}{dE_\nu}\sigma_{\text{inv}\beta}N_p\epsilon_{\text{eff}}. \tag{4.1}$$

Here, the positron energy in a given reaction E_{e^+} is related to the incident neutrino energy E_ν as,

$$E_{e^+} \approx (E_\nu - 1.3\,\text{MeV})(1 - E_\nu/m_p), \tag{4.2}$$

where m_p is the proton mass. The cross-section for the inverse β-decay process is denoted as $\sigma_{\text{inv}\beta}$, the number of reaction target protons is $N_p = 2.5 \times 10^{34}$ with 2×187 kton tanks of water[5] and the detector efficiency is denoted as ϵ_{eff}.

The cross-section for the inverse β-decay process for an incident neutrino energy E_ν is given by,

$$\sigma_{\text{inv}\beta} = 0.0952 \times 10^{-42}\,\text{cm}^2\,(E_\nu - 1.3)^2\left(1 - \frac{7E_\nu}{m_p}\right), \tag{4.3}$$

[5]The SK experiment has a fiducial volume of 22.5 kton, and thus has an order of magnitude less target protons than the HK experiment.

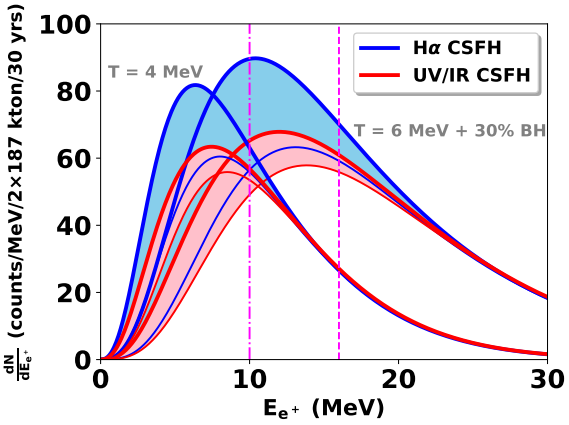

Figure 3. Expected positron spectrum with 30 years of observation at Hyper-Kamiokande with 2×187 kton tanks (fiducial volume) for different assumptions of the CSFH and the CC SNe temperature spectral parameter. The bands indicate contributions to the spectra from cosmic noon neutrinos ($1.5 \lesssim z \lesssim 3.5$). We have assumed a 70% net signal efficiency, taking into account various background reduction cuts on the data and assuming Gd loading at HK to tag accompanying neutrons in inverse β-decay events. The dashed vertical line indicates the analysis threshold of 16 MeV used in the 2011 DSNB search at Super-Kamiokande without Gd loading, whereas the dot-dashed vertical line indicates a threshold of 10 MeV which is expected with neutron tagging after Gd loading at both SK-Gd and HK.

where m_p and E_ν are both expressed in MeV. For the $\mathcal{O}(10)$ MeV range of neutrino energies that we are considering, the cross-section grows as $\sim E_\nu^2$, which leads to preferential detection of higher energy neutrinos.

Several sources of background must be rejected by applying cuts to the data, some of which are discussed in the next section. At SK these cuts reduced the efficiency of DSNB signal detection to a level of $\epsilon_{\rm eff} = 70$–80% [76].

In order to reject background and identify DSNB signal, it is useful to lower the threshold sensitivity of the detector by attempting to identify the neutron produced in the inverse β-decay reaction by tagging it. For the Super-Kamiokande detector, it has been proposed to load gadolinium (Gd) in the detector in a project known as SK-Gd [79, 117] (formerly GADZOOKS!). The basic idea is that the neutron capture efficiency on gadolinium is high and the subsequent de-excitation of Gd produces 8 MeV gamma cascade photons which inverse compton-scatter off of electrons in the detector and can be seen as a slightly-delayed, isotropic, secondary signal in the detector in addition to the primary prompt positron. Loading SK with 0.1% Gd by mass has been proposed, which would lead to a 90% tagging efficiency of genuine inverse β-decay events, slightly lowering the detector signal efficiency $\epsilon_{\rm eff}$ further. We will work with the assumption of 0.1% Gd loading at HK, and we take the overall positron signal efficiency to be $\epsilon_{\rm eff} = 70\%$ after Gd loading at HK.

Using eq. (4.1), we can now compute the expected positron spectrum under the assumptions of the UV/IR CSFH and the Hα CSFH. In figure 3, we show the expected positron spectrum at HK with 30 years of data assuming that both detectors are operational, for the scenarios where $T = 4$ MeV and $T = 6$ MeV with a 30% BH component. We show the contribution of positrons arising from cosmic noon ($1.5 \lesssim z \lesssim 3.5$) neutrinos by using shaded bands in the figure. We also tabulate the positron fractions at a specific energy/energy ranges arising from the cosmic noon in table 3. Since the detection probability of neutrinos increases as E_ν^2, this preferentially leads to detection of higher energy neutrinos. This detection bias

	Energy		Energy Range	
Temp	10 MeV	16 MeV	> 10 MeV	> 16 MeV
4 MeV	0.06 (0.11)	0.01 (0.01)	0.02 (0.04)	$< 1\%$
5 MeV	0.13 (0.22)	0.02 (0.05)	0.04 (0.08)	0.01 (0.02)
6 MeV	0.21 (0.32)	0.05 (0.10)	0.07 (0.14)	0.02 (0.05)
+10% BH	0.22 (0.34)	0.06 (0.12)	0.08 (0.15)	0.03 (0.06)
+20% BH	0.23 (0.35)	0.07 (0.14)	0.09 (0.16)	0.04 (0.08)
+30% BH	0.24 (0.37)	0.08 (0.16)	0.10 (0.18)	0.04 (0.09)
8 MeV	0.34 (0.47)	0.14 (0.24)	0.14 (0.24)	0.08 (0.14)

Table 3. Table of positron fractions arising from the cosmic noon ($1.5 \lesssim z \lesssim 3.5$) neutrinos at HK assuming the UV/IR CSFH for a given energy/energy range (columns). The rows correspond to different assumptions of the CC SNe temperature spectral parameter (T). Numbers in brackets indicate the corresponding fractions for the Hα CSFH. For the energy ranges of the right two columns, the upper limit of the range has been taken to be 25 MeV. Higher values of T would lead to a greater fraction of positrons arising from neutrinos from the cosmic noon. From an experimental point-of-view, measurement of the positron spectrum with a lower threshold will receive greater contributions from the cosmic noon neutrinos and thus will be more sensitive to the differences between the UV/IR and Hα CSFHs.

reduces the fraction of positrons created in the detector from neutrinos originating at the cosmic noon relative to positrons from lower redshift neutrinos. However, both the number of detected positrons and the fraction of positrons arising from cosmic noon neutrinos increases with higher values of the CC SN temperature parameter T. In figure 3, we also indicate thresholds for detection of the DSNB at SK/HK with and without Gd loading. We can clearly see from the figure that lowering the threshold by loading the detectors with Gd will significantly enhance sensitivity to positrons generated by neutrinos from the cosmic noon.

4.1 Background noise and detection threshold at Hyper-Kamiokande

In order to discriminate between CSFHs with different SFRDs at the cosmic noon, it is advantageous to detect neutrinos at low energies which have a greater contribution from high-redshift supernovae. However, there are two factors working against the detection of low-energy neutrinos. First, as already mentioned, the detection probability of neutrinos increases as E_ν^2, which preferentially leads to detection of higher energy neutrinos. Second, various backgrounds in the detector become important at low energies, overwhelming any chance of detecting the DSNB at energies $\lesssim 10$ MeV. While HK can in principle detect neutrinos down to 3 MeV of energy [77], in practice the detector has several sources of backgrounds in the energy range of interest, which make extraction of the DSNB signal difficult and restrict the range of energies over which the spectrum can be studied. Here, we list the primary sources of background at HK for the DSNB search:

1. Spallation from cosmic muons
2. Invisible muon background
3. Atmospheric $\bar{\nu}_e$, ν_e charged-current (CC) background
4. Atmospheric neutrino neutral current (NC) background
5. Reactor anti-neutrinos

Several of these sources of background can be significantly reduced by cuts on the data and by loading Gd in the detector to tag neutrons in genuine inverse β-decay reactions.

Spallation from cosmic muons can be reduced considerably by applying suitable spatial and temporal coincidence cuts to remove events associated with visible muons entering the detector. Loading Gd in the detector to tag neutrons significantly reduces the spallation background by many orders of magnitude. However, spallation products which are relatively long-lived and produce neutrons are harder to remove. In ref. [77], it was argued that of all spallation products, ^{9}Li with a half-life of 0.18 s is the most dominant residual spallation background. However, the relatively short lifetime of ^{9}Li allows for it to be rejected with 99.5% probability using coincidence cuts and this could possibly be improved further by optimizing the cuts.

Atmospheric muon neutrinos can produce muons in the detector via CC interactions, and these muons are typically below the Cherenkov threshold. The decay of these "invisible" muons produces electrons/positrons, which creates a background that can mimic the signal. The positron spectrum from this background is the well known Michel spectrum and can therefore be modelled very accurately, and is also distinct from the expected DSNB positron spectrum. Furthermore, with 0.1% Gd in the detector, the background from invisible muons can be further reduced by a factor of 5 [117].

Atmospheric $\bar{\nu}_e$ CC interactions produce a source of background which is indistinguishable from DSNB signal on an event-by-event basis, but fortunately has a very different spectrum compared to that expected from the DSNB. Atmospheric ν_e CC interactions produce electrons which are indistinguishable from positrons (and hence signal events) without Gd tagging, but can be reduced by looking for accompanying neutrons.

In addition, atmospheric neutrinos can interact elastically via neutral current interactions and some of these interactions may mimic the signal. The NC background can be reduced by Cerenkov angle cuts, but has still been shown to be important below positron energies of 20 MeV [76, 118].

Reactor $\bar{\nu}_e$s are another source of irreducible background below neutrino energies of ~ 10 MeV. While the background due to reactor neutrinos is overwhelming below 10 MeV, there is also a moderate tail from 10–15 MeV.

There are several other sources of background such as solar neutrinos and pions faking electrons, but these can be reduced to very low levels with solar angle and Cerenkov angle cuts respectively.

Thus, after application of the cuts and assuming neutron tagging with Gd loading at HK, the dominant surviving backgrounds in the energy range of interest are the ^{9}Li spallation background, the unresolved reactor neutrino tail, invisible muon spallation, atmospheric $\nu_e/\bar{\nu}_e$ CC events and atmospheric NC events that survive the cuts. The spectra of these individual backgrounds (combined for both detectors) and their sum as a function of reconstructed energy is shown in figure 4.

We have taken our ^{9}Li[6] and reactor neutrino backgrounds (assuming full reactor intensity) from the HK design report [77] and we have taken the NC background, the invisible muon background and the $\nu_e/\bar{\nu}_e$ CC backgrounds from an SK-Gd study [79] appropriately scaled up to the HK detector volume.

The spallation background decreases with increased overburden, and with a 1 km depth for the proposed Korean sites at Mt Bisul and Mt Bohyun, the spallation background is

[6] We have reduced the ^{9}Li background shown in figure 190 of ref. [77] by a factor of 4/6 based on a private correspondence with Hiroyuki Sekiya and Takatomi Yano.

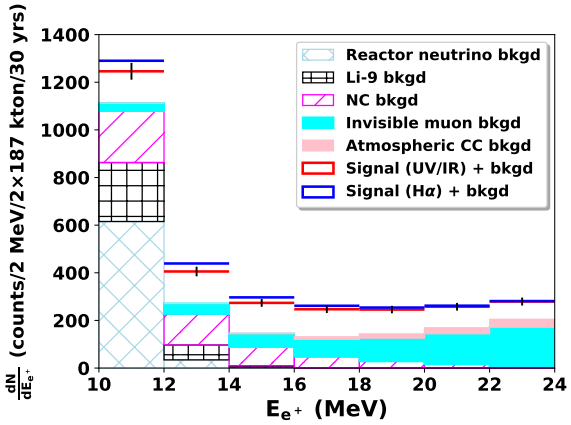

Figure 4. This histogram shows the expected backgrounds as a function of detected energy, combined from both HK sites with 30 years of data and assuming Gd loading. The combined DSNB signal with background is shown for both the UV/IR CSFH and the Hα CSFH assuming a CC SNe spectral parameter of $T = 6$ MeV with a 30% BH component. We have also shown the Poissonian ($\sqrt{N}$) errors for the UV/IR CSFH case for reference. We set 10 MeV as the lower threshold for our analysis to discriminate between the two different signal hypotheses, below which the reactor neutrino background overwhelms the signal.

expected to be a factor of ~ 4 smaller than at the Tochibora site [115]. Since there is no study yet of the reactor neutrino background at the Korean sites, we take a nominal assumption of the same reactor background at both the Tochibora and Korean sites. Other backgrounds, sourced by atmospheric neutrinos, are expected to be the same at both sites.

At Super-Kamiokande without Gd loading, the spallation background limited the search for DSNB down to 17.3 MeV neutrino energy [76]. The reduction of backgrounds with Gd loading allows for a lowering of the threshold energy of DSNB detection down to ~ 10 MeV, which is ultimately constrained by the reactor neutrino background. This reduction of the threshold will be extremely useful for studying neutrinos from the cosmic noon.

The cuts applied to the data to reduce the background also reduce the signal efficiency. While a detailed study of the reduced signal efficiency at a Gd loaded detector is not yet available, we assume a net efficiency of $\epsilon_{\rm eff} = 70\%$, which is consistent with an efficiency of 78% at SK [76] with a further reduction due to the 90% efficiency of neutron tagging.

4.2 Analysis and results

In figure 4, we show a histogram of the expected positron signal with background for the UV/IR and Hα CSFHs assuming a spectral parameter $T = 6$ MeV with a 30% BH component for the CC SNe temperature. The histogram represents expected data combined from both HK experiments over 30 years and also shows the relative contributions of different sources of background. We have also shown the Poissonian ($\sqrt{N}$) statistical error bars on the expected data assuming the UV/IR CSFH.

The difference between DSNB signal and background is prominent over a large energy range from 10–40 MeV. However, the difference between the two signal hypothesis is appreciable only below about 24 MeV and is more prominent at lower energies, where the difference in cosmic noon neutrino contributions is largest.

Given an assumption of the true CSFH. We can now ask two questions: a) How many years of data collection would it take to discover the DSNB signal? b) How many years of data collection would it take to rule out the alternative hypothesis for the CSFH? For concreteness, we will take the specific case of the assumption that the UV/IR CSFH is the correct one below.

To answer both the questions above, we need to define a null and an alternative hypothesis and a test statistic that will discriminate between them. For discovery potential, we take the null hypothesis to be background only and the alternative hypothesis to be background with DSNB signal assuming the UV/IR CSFH. For excluding the Hα CSFH, we take our null hypothesis to be background with DSNB signal assuming the Hα CSFH and our alternative hypothesis to be background with DSNB signal assuming the UV/IR CSFH. We define a chi-squared test statistic in the usual way as,

$$\chi^2 \equiv \sum_i \left(\frac{\text{obs}_i - \text{pred}_i}{\sigma_i} \right)^2 , \tag{4.4}$$

where obs_i is the observed (pseudo-)data in the i-th energy bin and pred_i is the mean predicted number of events under the null hypothesis in the same energy bin and $\sigma_i = \sqrt{\text{pred}_i}$, is the Poissonian fluctuation in the predicted number of events. Here, we have taken 2 MeV bins starting from an energy threshold of 10 MeV going up to 24 MeV, where the lower threshold is set by the reactor neutrino background, and the upper threshold is chosen in order to select a range where the two CSFHs yield the most different positron spectra.[7]

We then calculate the *average* chi-squared $\langle \chi^2 \rangle$ and its 1-σ fluctuation $\Delta\chi^2 \equiv \sqrt{\langle (\chi^2 - \langle \chi^2 \rangle)^2 \rangle}$. We will denote the expected mean number of events in the i-th bin under the null and alternative hypothesis as N_i and A_i, respectively. Then, fixing $\text{pred}_i = N_i$ and averaging over Poissonian, independent fluctuations of obs_i about the mean value of A_i, we obtain the following analytic expressions for $\langle \chi^2 \rangle$ and $\Delta\chi^2$,

$$\langle \chi^2 \rangle = \sum_i \left[\frac{A_i}{N_i} + \left(\frac{(A_i - N_i)^2}{N_i} \right) \right] , \tag{4.5}$$

$$\Delta\chi^2 = \sqrt{\sum_i \left[\frac{4A_i[(A_i - N_i)^2 + (A_i - N_i)] + 2A_i^2 + A_i}{N_i^2} \right]} . \tag{4.6}$$

Note that both N_i and A_i scale linearly with the number of years of data collection. We can now convert $\langle \chi^2 \rangle$ and its fluctuations $\langle \chi^2 \rangle \pm \Delta\chi^2$ into an average p-value $\langle p \rangle$ for discovery/exclusion and its fluctuation $\langle p \rangle \pm \Delta p$, for a given number of years of data collection.

We can then proceed to answer our questions above. The expected number of years required to discover the DSNB, assuming the UV/IR CSFH, would be the number of years needed for the average p-value to yield a 5-σ exclusion of the null hypothesis of background only, i.e. $\langle p \rangle = 6 \times 10^{-7}$. We can also find the fluctuation on the expected number of years for discovery by requiring $\langle p \rangle \pm \Delta p = 6 \times 10^{-7}$. Similarly, we can estimate the time required to rule out the alternative Hα CSFH at the 2-σ level ($p = 0.05$), and its uncertainty.

In table 4, we show the expected number of years to discovery of the DSNB signal and exclusion of the Hα CSFH assuming that the UV/IR CSFH is the right one under different assumptions of the CC SNe temperature parameter.

[7] For discovery of the DSNB it will be useful to extend the energy range of analysis to higher energies, but for simplicity, since we are focussed on cosmic noon neutrinos, we will use the same energy range for both discovery and exclusion analysis.

Temp	5-σ Discovery	2-σ Exclusion of Hα CSFH
4 MeV	$10.9^{+5.7}_{-3.9}$	> 200
5 MeV	$4.2^{+2.5}_{-1.7}$	> 200
6 MeV	$2.4^{+1.6}_{-1.0}$	$54.3^{+63.8}_{-35.3}$
+10% BH	$2.3^{+1.5}_{-1.0}$	$44.7^{+51.9}_{-28.8}$
+20% BH	$2.2^{+1.4}_{-1.0}$	$37.1^{+42.8}_{-23.7}$
+30% BH	$2.1^{+1.5}_{-0.9}$	$31.3^{+35.8}_{-19.8}$
8 MeV	$1.5^{+1.0}_{-0.7}$	$12.6^{+13.6}_{-7.6}$

Table 4. Left column: years needed for 5-σ discovery of the DSNB at HK loaded with Gd assuming that the UV/IR inferred CSFH is correct. Right column: years needed for 2-σ exclusion of the Hα CSFH assuming that the UV/IR inferred CSFH is correct. Rows correspond to different assumptions of the CC SNe temperature spectral parameter.

Temp	5-σ Discovery	2-σ Exclusion of UV/IR CSFH
4 MeV	$10.8^{+5.6}_{-3.9}$	> 200
5 MeV	$3.8^{+2.3}_{-1.5}$	> 200
6 MeV	$2.0^{+1.3}_{-0.9}$	$48.9^{+64.8}_{-34.9}$
+10% BH	$1.8^{+1.2}_{-0.8}$	$39.5^{+52.9}_{-28.5}$
+20% BH	$1.7^{+1.2}_{-0.8}$	$32.4^{+43.8}_{-23.5}$
+30% BH	$1.6^{+1.1}_{-0.7}$	$26.8^{+36.6}_{-19.7}$
8 MeV	$1.0^{+0.7}_{-0.4}$	$9.7^{+14.2}_{-7.6}$

Table 5. Left column: years needed for 5-σ discovery of the DSNB at HK loaded with Gd assuming that the Hα inferred CSFH is correct. Right column: years needed for 2-σ exclusion of the UV/IR CSFH assuming that the Hα inferred CSFH is correct. Rows correspond to different assumptions of the CC SNe temperature spectral parameter.

In table 5, we show the expected number of years to discovery of the DSNB signal and exclusion of the UV/IR CSFH assuming that the Hα CSFH is the right one under different assumptions of the CC SNe temperature parameter.

From the tables, we can see that for either the UV/IR or Hα assumption of the CSFH, discovery of the DSNB at HK loaded with Gd should take less than 10 years. Even with a low CC SNe temperature parameter of 4 MeV, the DSNB should be discoverable at HK, but the lower threshold sensitivity due to the addition of Gd will be critical for discovery with this relatively lower energy spectrum. Unsurprisingly, the discovery of the DSNB, assuming the Hα CSFH is correct, is expected to happen slightly sooner given the larger signal rates.

Now we come to the central question raised in the introduction: can the DSNB be used to probe the difference between the benchmark CSFHs inferred from UV/IR data and Hα data? We find that the DSNB signal at HK could potentially exclude the UV/IR or Hα CSFH hypothesis in favor of the other within 9.7–12.6 years of data collection in the scenario where the CC SNe temperature parameter $T = 8$ MeV. For slightly lower $T = 6$ MeV, even with a significant BH component ($\sim 30\%$), discriminating between the two hypothesis will

require ~ 30 years of data collection. For lower CC SNe temperatures, which are more in line with expectations from current SN simulations, discrimination of the different CSFHs will not be possible for any reasonable time-line and will require a next generation detector with a larger volume and/or a lower threshold sensitivity.

While our main analysis has focussed on HK loaded with Gd, we have also performed similar analyses for SK-Gd and HK without gadolinium (and assuming no neutron tagging, for e.g. by considering neutron capture on hydrogen) taking into account appropriate backgrounds for each detector. We attempted to understand whether the discovery of the DSNB and the rejection of the alternative CSFH can be made over a 30-year time span.

For SK-Gd, we have included reactor neutrino backgrounds and ^{9}Li backgrounds in addition to the backgrounds considered in ref. [79] and we find that 5-σ discovery of the DSNB is possible for the benchmark scenario where $T = 8\,\mathrm{MeV}$ with a mean time of 23.8 (15.3) years and $T = 6\,\mathrm{MeV}$ with a mean time between 33.4–38.9 (24.7–31.2) years for the UV/IR (Hα) CSFH hypothesis, with the exact value in the latter case depending on the assumed BH component. However exclusion of the alternative CSFH will not be possible over a 30-year time span even for such high temperatures.

For HK without Gd, we have considered an analysis threshold of 16 MeV to reject the increased spallation background that would be present. The higher threshold would imply a lower sensitivity to cosmic noon neutrinos. We find that discovery is possible for $T = 8\,\mathrm{MeV}$ with a mean time of 7.9 (5.9) years, $T = 6\,\mathrm{MeV}$ with a mean time between 12.5–15.8 (10.5–14.4) years, and also for the $T = 5\,\mathrm{MeV}$ scenario with a mean time of 32.3 years. However, HK without Gd will not be sensitive to the difference between the UV/IR and Hα CSFHs.

Thus in order to be sensitive to cosmic noon neutrinos, it is crucial that HK is loaded with Gd to allow a study of the spectrum of CC SNe down to $\sim 10\,\mathrm{MeV}$. *Both the larger detector volume of HK and the lowered threshold with Gd loading are required for detection and characterization of the CSFH using the DSNB.*

5 Summary and conclusions

Understanding galaxy formation and evolution is one of the open frontier problems in modern cosmology and is a critical step towards a better understanding of the behaviour of dark matter on small scales. One of the key observational inputs needed to study galaxy formation and evolution is knowledge of the cosmic star formation history.

Measurement of the DSNB spectrum has the potential to allow for detailed inferences of the CSFH. In this work, we were particularly interested in the sensitivity of DSNB measurements at the Hyper-Kamiokande experiment to the *cosmic noon*, which is the epoch of peak star formation between $1.5 \lesssim z \lesssim 3.5$.

We examined inferences of the CSFH from Hα data and compared it to the CSFH inferred from UV/IR data and found that the best fit CSFH in the former case was larger by a factor of ~ 3 near the cosmic noon. While this discrepancy is not statistically significant, we used the two different best-fit CSFHs to construct benchmark hypotheses to see if HK could be sensitive to the difference between them.

Since the spectrum of cosmologically averaged CC SNe is not yet known, for our analysis, we selected a set of benchmark CC SNe spectra which differed only in their choice of temperature parameter (T), with higher temperatures leading to a slightly higher energy spectrum. Numerical simulations, possibly calibrated to future observations of local SNe (within 10 Mpc), could solidify our understanding of this spectrum within the next decade or two.

Since cosmological neutrinos are redshifted, the low energy DSNB is more sensitive to differences in the SFRD at the cosmic noon. However, there are several challenges with detection of these cosmic noon neutrinos:

- The detection probability of neutrinos scales as E_ν^2, which suppresses the rate of lower energy neutrino signals relative to higher energy neutrinos.
- Various detector backgrounds make the study of low energy neutrinos challenging.

We then studied the potential of the next-generation Hyper-Kamiokande detector to characterize the spectrum of the DSNB and to discriminate between different CSFHs. The baseline design for HK only looks for positrons produced in inverse β-decay reactions and will be limited in its low energy threshold to $\sim 16\,\mathrm{MeV}$ due to spallation backgrounds. However, loading HK with 0.1% gadolinium by mass to tag accompanying neutrons can lower the spallation background (and other backgrounds) significantly, lowering the threshold to $\sim 10\,\mathrm{MeV}$, below which reactor neutrino background overwhelms any signal.

We found that depending on the CC SNe spectral parameters, discovery of the DSNB is almost assured over a 10-year time scale, and possibly even within 1–2 years of operation of HK loaded with gadolinium. Our main result shows that discrimination of the CSFH inferred from UV/IR data versus that inferred from Hα data should be possible with 10–30 years of operation, assuming higher CC SNe temperature parameters ($T = 8\,\mathrm{MeV}$ or $T = 6\,\mathrm{MeV}$ with a 30% BH component). However, for other benchmark scenarios with lower temperature and in particular for $T = 4\,\mathrm{MeV}$ which seems to be indicated by CC SN simulations, we find that although the DSNB should be discoverable, the spectrum will be too low in energy for HK to be sensitive to the cosmic noon neutrinos and it will not be able to discriminate between the different CSFHs on a reasonable timescale. We also found that discrimination of the two CSFHs will not be possible at SK-Gd or at HK without Gd loading.

Our results have only taken into account statistical uncertainties and we have ignored systematic uncertainties which might affect our conclusions. Some of these important systematic uncertainties would be the uncertainty on various low energy backgrounds, and crucially, uncertainties on the to-be-determined CC SNe spectral parameters.

Calibration of numerical simulations of CC SNe can be accomplished using galactic SNe at current detectors (assuming we are lucky enough to see an explosion) or using observations of nearby SNe, which would require large volume detectors like HK itself. In the latter case, characterizing the spectrum using HK data would require analysis and extraction of local SNe spectral information, only after which, one can use the simultaneously collected DSNB data to discriminate between the two CSFHs. Thus, unless we are fortunate enough to see a galactic SN explosion soon, discrimination of the two CSFHs will require waiting until sufficient data is gathered to understand the CC SN spectrum reliably.

In conclusion, the ability of a next-generation, large-volume detector like HK to draw inferences of the detailed CSFH, especially near the cosmic noon, would be a significant milestone for neutrino astrophysics.

In order to be sensitive to the cosmic noon neutrinos for the broadest possible set of CC SNe spectra, there is a clear need for Hyper-Kamiokande to go to lower thresholds and this can be accomplished via gadolinium loading. Another possible improvement is to attempt to lower thresholds for the second detector could be to build it with more overburden to reduce the cosmic ray spallation background and/or to build it further from nuclear reactors to reduce the reactor neutrino background. We hope that future detector commissioning plans for HK will take into account these ideas given the major science goal presented in this work.

Acknowledgments

The authors acknowledge very helpful correspondence with Hiroyuki Sekiya and Takatomi Yano regarding backgrounds at HK. The authors thank Varun Bhalerao and Basudeb Dasgupta for enlightening discussions and helpful comments on the draft. VR is supported by a DST-SERB Early Career Research Award (ECR/2017/000040) and an IITB-IRCC seed grant.

A SFRD data

In this appendix, we discuss the Hα data that we have used when performing our fit to the CSFH shown in figure 1. Several corrections have to be made to the published data and errors and we describe the reasons for these corrections factors below. We present the final corrected SFRD in table 6 along with the references from which we have taken the data. Data near the peak of cosmic noon is indicated in bold font in the table. We have also presented in the table some of the key assumptions made when determining the SFRD in the original reference, along with some of the features of the surveys, such as sample area and number of galaxies used.

Deriving the SFRD from Hα observations in a given survey involves several steps. First, the Hα flux (or equivalent width) observed from a given galaxy has to be converted to the intrinsic Hα luminosity ($L^{\rm int}_{H\alpha}$). This conversion involves distance determination along with dust extinction and AGN corrections as the major astrophysical inputs. Since different studies make different assumptions for how these factors are computed, the data must be self-consistently recalibrated to use the same astrophysical assumptions.

The distance determination is made by using the observed redshift of the galaxy and a cosmological model assumption. We have used the correction factors in the appendix of Gunawardhana et al. [64] to correct older studies which did not use the ΛCDM cosmology. Dust extinction corrections can sometimes be estimated by looking at Balmer decrements, that is the relative fluxes of the Hβ and Hα lines. For high redshift galaxies however, such a measurement is typically not feasible. Using Balmer decrement measurements of low redshift SDSS galaxies, Garn and Best [119] explored how various factors such as star formation rate, metallicity, and stellar mass can affect the Hα extinction. The results of this study could in principle be applied to high redshift galaxies to obtain reliable estimates of their extinction factors. However, for the studies that we have considered, each uses different assumptions for the estimate of the dust extinction correction which we have listed in table 6. A few studies have not corrected for dust extinction at all. We have not attempted to recorrect different extinction factors, except for data which does not include an extinction correction. For such data, we include a standard extinction factor of 1 mag as is often assumed in the literature [52, 120] and which is consistent with the average value seen in [119] at low redshifts. AGN corrections are in the 5–15% range and have a relatively less significant effect on the SFRDs, so we do not correct for different assumptions of the AGN correction between different studies.

Once the intrinsic luminosities of all galaxies in a survey are obtained, the galaxy count must be corrected for survey incompleteness. This is done by fitting the observed luminosities to a luminosity function (LF), denoted as $\Phi(L)$, defined as the number of galaxies per unit volume per unit luminosity, to extrapolate the galaxy count to include dimmer galaxies. These galaxies would be missed by the survey but could contribute significantly to the

estimated SFRD at a given redshift due to their large numbers. This determination of the LF must be made separately in different redshift bins. The choice of luminosity function and its limits impacts the estimated SFRD. Different studies use different assumptions of the luminosity function and the limits, but this correction is challenging to make when the assumed functions are different. We do not make a correction for different assumptions of the luminosity function.

For an inferred intrinsic luminosity, the star formation rate (SFR) of a given galaxy can be found by applying a conversion factor based on a population synthesis model,

$$\text{SFR (in } M_\odot/\text{year}) = C \times L^{\text{int}}_{H\alpha} \text{ (in erg/s)}. \tag{A.1}$$

We recalibrate all data to use the Kennicutt [121] conversion factor $C = 7.9 \times 10^{-42}$, which assumes a Salpeter IMF with masses between 0.1 $M_\odot$–100 $M_\odot$ and solar metallicity. This choice is important for consistency with the inference made from UV/IR data which also assumes the same IMF.

From the inferred luminosity function at a given redshift and the conversion factor, the SFRD at any redshift can be obtained as,

$$R^{H\alpha}_{\text{SF}}(z) = \int_{L\text{min}}^{L\text{max}} dL\, \Phi(L, z) \times \text{SFR}(L), \tag{A.2}$$

where $\text{SFR}(L) = C \times L$.

While most of the references report only statistical errors on the SFRD, a few of them account for some systematic uncertainties too. When performing any recalibration of the reported SFRDs, we have rescaled the reported errors by preserving the fractional errors on the original SFRD measurements. For the cases in which the reported errors are asymmetric, we have averaged upper and lower errors.

Some notes about the data. Gunawardhana et al. [64] has the most precise data in the low redshift regime and strongly influences the fit at low redshift. However, the data of ref. [64] involve both GAMA and SDSS samples. SDSS (low redshift survey, z $\lesssim$ 0.2) has a brighter magnitude cut than other surveys like GAMA. This prevents optically faint high-SFR galaxies from entering the SDSS sample, resulting in lower values of estimated SFRD. The assertion is further supported by the lack of evolution of SDSS luminosity function with redshift [64]. Therefore, we have omitted the SDSS SFRD values given in this reference.

Except for Gunawardhana et al. [64] and Pascual et al. [36], all references use a Schechter [122] luminosity function. Gunawardhana et al. [64] uses a Saunders [123] luminosity function, while Pascual et al. [36] uses their own functional form.

Stroe and Sobral [65], Gunawardhana et al. [64], Westra et al. [60], Brinchmann et al. [42] and Gallego et al. [29] have assumed Chabrier IMF [124], Baldry & Glazebrook IMF [125], Chabrier IMF, Kroupa IMF [126], and Scalo IMF [127], respectively. Tresse and Maddox [31] and Gallego et al. [29] have used a Salpeter IMF, but they have taken the stellar mass-range limits between 0.1 and 125 $M_\odot$. We have recalibrated the reported SFRDs of these references to the Kennicutt [121] conversion factor based on Salpeter IMF and stellar mass-range limits between 0.1 and 100 $M_\odot$.

Reference	**z**	**Sample Area**	**Galaxy Count**	**Extinction Correction**	**AGN Correction**	C (10^{-42})	**cf.**	**SFRD**	**SFRD Error**
Harish 2020 [69]	0.62	1.5 deg^2	241	1 mag	11%	7.9	1	0.041	0.008
Khostovan 2020 [68]	0.47	3 deg^2	1577	1 mag	10%	7.9	1	0.023	0.002
Coughlin 2018 [67]	0.62	1.1 deg^2 × 5	847	galaxies individually corrected according to their luminosity [128]	11%	7.9	1	0.043	0.008
Sobral 2015 [66]	0.81	10 deg^2	3471	1 mag	10%	7.9	1	0.086	0.003
Stroe 2015 [65]	0.2	26 deg^2	220	1 mag	15%	4.4	1.8	0.017	0.0014
Sobral 2013 [28]	**2.23**	2 deg^2	807	1 mag	10%	7.9	1	**0.21**	0.025
	1.47		515		10%			**0.13**	0.02
	0.84		637		15%			0.1	0.015
	0.4		1742		15%			0.03	0.01
Gunwardhan 2013				Balmer decrements [129]		2.9	2.7		
GAMA [64]	0.3	48 deg^2 × 3	11675		9%			0.035	0.0003
	0.2							0.021	0.0002
	0.127							0.022	0.0002
	0.05							0.023	0.0005
Sobral 2012 [63]	**1.47**	0.7 deg^2	200	1 mag	15%	7.9	1	**0.16**	0.05
Tadaki 2011 [62]	**2.2**	56 arcmin^2	11	1 mag	none	7.9	1	**0.31**	0.16*
Ly 2011 [61]	0.8	0.82 deg^2	394	galaxies individually corrected according to their luminosity [128]	11%	7.9	1	0.1	0.04
Hayes 2010 [58]	**2.2**	0.016 deg^2	55	1 mag	none	7.9	1	**0.2**	0.09
Dale 2010 [59]	0.4	1.11 deg^2	91	1 mag	none	7.9	1	0.02	0.002
	0.32	4.13 deg^2	438					0.02	0.001
	0.24	4.03 deg^2	424					0.01	0.001
	0.16	4.19 deg^2	214					0.01	0.001
Westra 2010 [60]	0.34	4 deg^2	848	galaxies individually	5.2%	7.9	1	0.015	0.003
	0.25		1268	corrected according	5.3%			0.015	0.004
	0.15		1127	to their luminosity [128]	6.6%			0.012	0.003
	0.055		322		5.9%			0.006	0.003
Karachentsev 2010 [57]	0.001	0.002 deg^2	52	galaxies individually corrected according to their axial ratio & rotation velocity of galaxy [130]	none	1.8	4.4	0.088	0.01
Shim 2009 [56]	**1.6**	104 arcmin^2	80	none	none	7.9	2.51	**0.7**	0.4
	1.4							**0.3**	0.1
	1.1							0.2	0.1
Sobral 2009 [55]	0.845	1.4 deg^2	743	1 mag	15%	7.9	1	0.15	0.01
Geach 2008 [52]	**2.23**	0.62 deg^2	55	1 mag	15%	7.9	1	**0.25**	0.17
Villar 2008 [48]	0.84	0.17 deg^2	165	1.45 mag	none	7.9	1	0.2	0.03
Westra 2008 [53]	0.24	0.5 deg^2		0.96 mag	5%	7.9	1		
CDFS			372					0.01	0.002
S11			335					0.006	0.002
Morioka 2008 [54]	0.24	875 arcmin^2	575	1 mag	none	7.9	1	0.035	0.02
Shioya 2008 [50]	0.24	5540 arcmin^2	980	galaxies individually corrected according to their R_C-band magnitude [131]	15%	7.9	1	0.018	0.006

* Taken from Gunawardhana et al. [64].

Dale 2008 [51]	0.24 0.16	2 deg^2	306	1 mag	none	7.9	1	0.019 0.011	0.008 0.007
James 2008 [49]	0.005	-	327	1.1 mag	none	7.9	1	0.02	0.001
Ly 2007 [47]	0.4 0.24 0.08	0.24 deg^2	391 259 318	galaxies individually corrected according to their luminosity [128]	none	7.9	1	0.02 0.01 0.01	0.008* 0.004* 0.01*
Doherty 2006 [45]	1	100 arcmin^2	38	none	9.5 %	7.9	2.51	0.1	0.02*
Hanish 2006 [46]	0.06	-	110	0.82 mag	none	7.9	1	0.02	0.004
Pascual 2005 [44]	0.4 0.24	-	-	1 mag	none	-	-	0.06* 0.04*	0.05* 0.03*
Glazebrook 2004 [43]	0.38	20 arcmin^2	41	0.8 mag	none	7.9	1	0.02	0.008
Brinchmann 2004 [42]	0.1	-	-	1 mag	15 %	5.25	1.5	0.03	0.004
Nakamura 2004 [41]	0.05	229.7 deg^2	665	0.81 mag	16 %	7.4	1.05	0.016	0.005
Hippelein 2003 [40]	0.25	100 arcmin^2 $\times$ 4	92	0.8 mag	none	7.9	1	0.02	0.006
Fujita 2003 [39]	0.24	706 arcmin^2	348	1 mag	15 %	7.9	1	0.04	0.009
Perez 2003 [38]	0.026	-	79	Balmer decrements [129]	none	8.2	0.96	0.03	0.006
Tresse 2002 [37]	0.73	30 arcmin^2	30	1 mag	15 %	7.9	0.88	0.09	0.01
Pascual 2001 [36]	0.242	0.19 deg^2	52	1 mag	8 %	7.9	1.4	0.05	0.01
Hopkins 2000 [35]	**1.25**	4.4 arcmin^2	37	none	none	7.9	1.43	**0.24**	0.04*
Yan 1999 [33]	**1.3**	64 arcmin^2	-	none	none	7.9	2.1	**0.3**	0.08
Glazebrook 1999 [32]	0.885	-	13	0.6 mag	none	7.9	0.89	0.1	0.04
Pettini 1998 [30]	3	-	5	none	none	8.93	0.78	0.3*	0.1*
Tresse 1998 [31]	0.2	0.12 deg^2	138	1 mag	none	7.1	1.3	0.025	0.002
Gallego 1995 [29]	0.045	471.4 deg^2	264	none	none	1.064	1	0.01	0.006

* Taken from Gunawardhana et al. [64].

Table 6. Table of Hα data. Columns give the original reference that the data was taken from, redshift (z), sample area, galaxy count, along with the extinction factor, AGN correction factor, and luminosity-to-SFR conversion factor C used in the original reference. Our correction factors, which we have multiplied with the original reported SFRD to recalibrate to the assumptions described in the text, are under the column labelled "cf.". The last two columns contain our recalibrated SFRD at the corresponding redshift and the corresponding error (both in units of $M_\odot\,\mathrm{Mpc}^{-3}\,\mathrm{yr}^{-1}$). Data near the peak of cosmic noon is indicated in bold font.

References

[1] Planck collaboration, *Planck 2018 results. VI. Cosmological parameters*, *Astron. Astrophys.* **641** (2020) A6 [arXiv:1807.06209] [inSPIRE].

[2] W.J. Percival, *Large Scale Structure Observations*, in *186th Course of International School of Physics 'Enrico Fermi': New Horizons for Observational Cosmology. Vol. 186*, Rome Italy (2013), pg. 101 [arXiv:1312.5490] [inSPIRE].

[3] J. Silk, *Challenges in Cosmology from the Big Bang to Dark Energy, Dark Matter and Galaxy Formation*, *JPS Conf. Proc.* **14** (2017) 010101 [arXiv:1611.09846] [inSPIRE].

[4] M. Vogelsberger, F. Marinacci, P. Torrey and E. Puchwein, *Cosmological Simulations of Galaxy Formation*, *Nature Rev. Phys.* **2** (2020) 42 [arXiv:1909.07976] [inSPIRE].

[5] S.-H. Oh, W.J.G. de Blok, E. Brinks, F. Walter and R.C. Kennicutt, Jr, *Dark and luminous matter in THINGS dwarf galaxies*, *Astron. J.* **141** (2011) 193 [arXiv:1011.0899] [INSPIRE].

[6] M. Rocha et al., *Cosmological Simulations with Self-Interacting Dark Matter I: Constant Density Cores and Substructure*, *Mon. Not. Roy. Astron. Soc.* **430** (2013) 81 [arXiv:1208.3025] [INSPIRE].

[7] A.H.G. Peter, M. Rocha, J.S. Bullock and M. Kaplinghat, *Cosmological Simulations with Self-Interacting Dark Matter II: Halo Shapes vs. Observations*, *Mon. Not. Roy. Astron. Soc.* **430** (2013) 105 [arXiv:1208.3026] [INSPIRE].

[8] J. Zavala, M. Vogelsberger and M.G. Walker, *Constraining Self-Interacting Dark Matter with the Milky Way's dwarf spheroidals*, *Mon. Not. Roy. Astron. Soc.* **431** (2013) L20 [arXiv:1211.6426] [INSPIRE].

[9] M. Boylan-Kolchin, J.S. Bullock and M. Kaplinghat, *Too big to fail? The puzzling darkness of massive Milky Way subhaloes*, *Mon. Not. Roy. Astron. Soc.* **415** (2011) L40 [arXiv:1103.0007] [INSPIRE].

[10] M. Vogelsberger, J. Zavala and A. Loeb, *Subhaloes in Self-Interacting Galactic Dark Matter Haloes*, *Mon. Not. Roy. Astron. Soc.* **423** (2012) 3740 [arXiv:1201.5892] [INSPIRE].

[11] J.S. Bullock, A.V. Kravtsov and D.H. Weinberg, *Reionization and the abundance of galactic satellites*, *Astrophys. J.* **539** (2000) 517 [astro-ph/0002214] [INSPIRE].

[12] A.J. Benson, C.S. Frenk, C.G. Lacey, C.M. Baugh and S. Cole, *The effects of photoionization on galaxy formation. 2. Satellites in the local group*, *Mon. Not. Roy. Astron. Soc.* **333** (2002) 177 [astro-ph/0108218] [INSPIRE].

[13] F. Governato et al., *Cuspy No More: How Outflows Affect the Central Dark Matter and Baryon Distribution in Lambda CDM Galaxies*, *Mon. Not. Roy. Astron. Soc.* **422** (2012) 1231 [arXiv:1202.0554] [INSPIRE].

[14] A. Del Popolo and M. Le Delliou, *Small scale problems of the ΛCDM model: a short review*, *Galaxies* **5** (2017) 17 [arXiv:1606.07790] [INSPIRE].

[15] P. Madau and M. Dickinson, *Cosmic Star Formation History*, *Ann. Rev. Astron. Astrophys.* **52** (2014) 415 [arXiv:1403.0007] [INSPIRE].

[16] M.-M. Mac Low, *From Gas to Stars Over Cosmic Time*, *Science* **340** (2013) 17.

[17] L. Hernquist and V. Springel, *An analytical model for the history of cosmic star formation*, *Mon. Not. Roy. Astron. Soc.* **341** (2003) 1253 [astro-ph/0209183] [INSPIRE].

[18] J. Schaye et al., *The EAGLE project: Simulating the evolution and assembly of galaxies and their environments*, *Mon. Not. Roy. Astron. Soc.* **446** (2015) 521 [arXiv:1407.7040] [INSPIRE].

[19] A. Pillepich et al., *Simulating Galaxy Formation with the IllustrisTNG Model*, *Mon. Not. Roy. Astron. Soc.* **473** (2018) 4077 [arXiv:1703.02970] [INSPIRE].

[20] C. Conroy, *Modeling the Panchromatic Spectral Energy Distributions of Galaxies*, *Ann. Rev. Astron. Astrophys.* **51** (2013) 393 [arXiv:1301.7095] [INSPIRE].

[21] E.E. Salpeter, *The Luminosity function and stellar evolution*, *Astrophys. J.* **121** (1955) 161 [INSPIRE].

[22] J. Moustakas, R.C. Kennicutt, Jr. and C.A. Tremonti, *Optical star-formation rate indicators*, *Astrophys. J.* **642** (2006) 775 [astro-ph/0511730] [INSPIRE].

[23] D. Spergel et al., *Wide-Field InfrarRed Survey Telescope-Astrophysics Focused Telescope Assets WFIRST-AFTA 2015 Report*, arXiv:1503.03757 [INSPIRE].

[24] J. Green et al., *Wide-Field InfraRed Survey Telescope (WFIRST) Final Report*, arXiv:1208.4012 [INSPIRE].

[25] EUCLID collaboration, *Euclid Definition Study Report*, arXiv:1110.3193 [INSPIRE].

[26] L. Pozzetti et al., *Modelling the number density of Hα emitters for future spectroscopic near-IR space missions*, *Astron. Astrophys.* **590** (2016) A3 [arXiv:1603.01453] [INSPIRE].

[27] J.P. Gardner et al., *The James Webb Space Telescope*, *Space Sci. Rev.* **123** (2006) 485 [astro-ph/0606175] [INSPIRE].

[28] D. Sobral et al., *A large Hα survey at $z = 2.23$, 1.47, 0.84 and 0.40: the 11 Gyr evolution of star-forming galaxies from HiZELS*, *Mon. Not. Roy. Astron. Soc.* **428** (2013) 1128 [arXiv:1202.3436] [INSPIRE].

[29] J. Gallego, J. Zamorano, A. Aragon-Salamanca and M. Rego, *The Current star formation rate of the local universe*, *Astrophys. J. Lett.* **455** (1995) L1 [astro-ph/9510061] [INSPIRE].

[30] M. Pettini, M. Kellogg, C.C. Steidel, M. Dickinson, K.L. Adelberger and M. Giavalisco, *Infrared Observations of Nebular Emission Lines from Galaxies at $Z \simeq 3$*, *Astrophys. J.* **508** (1998) 539 [astro-ph/9806219] [INSPIRE].

[31] L. Tresse and S.J. Maddox, *The H-alpha luminosity function and star formation rate at $z \sim 0.2$*, *Astrophys. J.* **495** (1998) 691 [astro-ph/9709240] [INSPIRE].

[32] K. Glazebrook et al., *Measurement of star-formation rate from H-alpha in field galaxies at $z = 1$*, *Mon. Not. Roy. Astron. Soc.* **306** (1999) 843 [astro-ph/9808276] [INSPIRE].

[33] L. Yan et al., *The h alpha luminosity function and global star formation rate from redshifts of one to two*, *Astrophys. J. Lett.* **519** (1999) L47 [astro-ph/9904427] [INSPIRE].

[34] A.F.M. Moorwood, P.P. van der Werf, J.G. Cuby and T. Oliva, *Halpha emitting galaxies and the cosmic star formation rate at $Z = 2.2$*, *Astron. Astrophys.* **362** (2000) 9 [astro-ph/0009010] [INSPIRE].

[35] A.M. Hopkins, A.J. Connolly and A.S. Szalay, *Star formation in galaxies between $0.7 < Z < 1.8$*, *Astron. J.* **120** (2000) 2843 [astro-ph/0009073] [INSPIRE].

[36] S. Pascual, J. Gallego, A. Aragon-Salamanca and J. Zamorano, *H-alpha emitting galaxies and the star formation rate density at $z \simeq 0.24$*, *Astron. Astrophys.* **379** (2001) 798 [astro-ph/0110177] [INSPIRE].

[37] L. Tresse, S.J. Maddox, O. Le Fèvre and J.-G. Cuby, *The Hα luminosity function and star formation rate up to $z \sim 1$*, *Mon. Not. Roy. Astron. Soc.* **337** (2002) 369.

[38] P.G. Pérez-González, J. Zamorano, J. Gallego, A. Aragon-Salamanca and A.G. de Paz, *Spatial analysis of the H-alpha emission in the local star-forming UCM galaxies*, *Astrophys. J.* **591** (2003) 827 [astro-ph/0303323] [INSPIRE].

[39] S.S. Fujita et al., *The H alpha luminosity function and star formation rate at $Z = 0.24$ based on Subaru deep imaging data*, *Astrophys. J. Lett.* **586** (2003) L115 [astro-ph/0302473] [INSPIRE].

[40] H. Hippelein et al., *Star forming rates between $z = 0.25$ and $z = 1.2$ from the CADIS emission line survey*, *Astron. Astrophys.* **402** (2003) 65 [astro-ph/0302116] [INSPIRE].

[41] O. Nakamura, M. Fukugita, J. Brinkmann and D.P. Schneider, *The H-alpha luminosity function of morphologically classified galaxies in the Sloan Digital Sky Survey*, *Astron. J.* **127** (2004) 2511 [astro-ph/0312519] [INSPIRE].

[42] J. Brinchmann et al., *The Physical properties of star forming galaxies in the low redshift universe*, *Mon. Not. Roy. Astron. Soc.* **351** (2004) 1151 [astro-ph/0311060] [INSPIRE].

[43] K. Glazebrook, J. Tober, S. Thomson, J. Bland-Hawthorn and R. Abraham, *Cosmic Star Formation History to $z = 1$ from a Narrow Emission Line-selected Tunable-Filter Survey*, *Astron. J.* **128** (2004) 2652.

[44] S. Pascual, *The Star formation rate density of the Universe at $z = 0.24$ and $z = 0.4$ from H-α*, *Publ. Astron. Soc. Pac.* **117** (2005) 120.

[45] M. Doherty, A. Bunker, R. Sharp, G. Dalton, I. Parry and I. Lewis, *The star formation rate at redshift one: H-α spectroscopy with CIRPASS*, *Mon. Not. Roy. Astron. Soc.* **370** (2006) 331 [astro-ph/0604584] [INSPIRE].

[46] D.J. Hanish et al., *The Survey for Ionization in Neutral Gas Galaxies. 2. The Star Formation Rate Density of the Local Universe*, *Astrophys. J.* **649** (2006) 150 [astro-ph/0604442] [INSPIRE].

[47] C. Ly et al., *The Luminosity Function and Star Formation Rate between Redshifts of 0.07 and 1.47 for Narrow-band Emitters in the Subaru Deep Field*, *Astrophys. J.* **657** (2007) 738 [astro-ph/0610846] [INSPIRE].

[48] V. Villar et al., *The Halpha-based Star Formation Rate Density of the Universe at $z = 0.84$*, *Astrophys. J.* **677** (2008) 169 [arXiv:0712.4150] [INSPIRE].

[49] P.A. James, J.H. Knapen, N.S. Shane, I.K. Baldry and R.S. de Jong, *The H alpha Galaxy Survey. IV. Star formation in the local Universe*, *Astron. Astrophys.* **482** (2008) 507 [arXiv:0802.4421] [INSPIRE].

[50] Y. Shioya et al., *The Hα Luminosity Function and Star Formation Rate at $z \approx 0.24$ in the Cosmos 2 Square-Degree Field*, *Astrophys. J. Suppl.* **175** (2008) 128 [arXiv:0709.1009] [INSPIRE].

[51] D.A. Dale et al., *The Wyoming Survey for H-α. I. Initial Results at $z \sim 0.16$ and 0.24*, *Astron. J.* **135** (2008) 1412.

[52] J.E. Geach et al., *HiZELS: a high redshift survey of H-alpha emitters. I: the cosmic star-formation rate and clustering at $z = 2.23$*, *Mon. Not. Roy. Astron. Soc.* **388** (2008) 1473 [arXiv:0805.2861] [INSPIRE].

[53] E. Westra and D.H. Jones, *Star Formation Density and H-alpha Luminosity Function of an Emission Line Selected Galaxy Sample at $z \sim 0.24$*, *Mon. Not. Roy. Astron. Soc.* **383** (2008) 339 [arXiv:0710.1140] [INSPIRE].

[54] T. Morioka, A. Nakajima, Y. Taniguchi, Y. Shioya, T. Murayama and S.S. Sasaki, *Star-Forming Galaxies at $z = 0.24$ in the Subaru Deep Field and the Sloan Digital Sky Survey*, *Publ. Astron. Soc. Jap.* **60** (2008) 1219 [arXiv:0807.0101] [INSPIRE].

[55] D. Sobral et al., *HiZELS: a high redshift survey of H-alpha emitters. II: the nature of star-forming galaxies at $z = 0.84$*, *Mon. Not. Roy. Astron. Soc.* **398** (2009) 75 [arXiv:0901.4114] [INSPIRE].

[56] H. Shim et al., *Global Star Formation Rate Density over $0.7 < z < 1.9$*, *Astrophys. J.* **696** (2009) 785 [arXiv:0902.0736] [INSPIRE].

[57] I.D. Karachentsev and S.S. Kaisin, *More galaxies in the Local Volume imaged in H-alpha*, *Astron. J.* **140** (2010) 1241 [arXiv:1010.2053] [INSPIRE].

[58] M. Hayes, D. Schaerer and G. Ostlin, *The H-alpha luminosity function at redshift 2.2: A new determination using VLT/HAWK-I*, *Astron. Astrophys.* **509** (2010) L5 [arXiv:0912.3267] [INSPIRE].

[59] D.A. Dale et al., *The Wyoming Survey for H-alpha. III. H-alpha Luminosity Functions at $z \sim 0.16$, 0.24, 0.32, and 0.40*, *Astrophys. J. Lett.* **712** (2010) L189 [arXiv:1003.0463] [INSPIRE].

[60] E. Westra, M.J. Geller, M.J. Kurtz, D.G. Fabricant and I. Dell'Antonio, *Evolution of the Halpha luminosity function*, *Astrophys. J.* **708** (2010) 534 [arXiv:0911.0417] [INSPIRE].

[61] C. Ly et al., *The H-alpha Luminosity Function and Star-Formation Rate Volume Density at $z = 0.8$ from the NEWFIRM H-alpha Survey*, *Astrophys. J.* **726** (2011) 109 [arXiv:1011.2759] [INSPIRE].

[62] K.-i. Tadaki, T. Kodama, Y. Koyama, M. Hayashi, I. Tanaka and C. Tokoku, *Cosmic Star Formation Activity at $z = 2.2$ Probed by H-alpha Emission Line Galaxies*, *Publ. Astron. Soc. Jap.* **63** (2011) 437 [arXiv:1012.4860] [INSPIRE].

[63] D. Sobral, P.N. Best, Y. Matsuda, I. Smail, J.E. Geach and M. Cirasuolo, *Star formation at $z = 1.47$ from HiZELS: an Hα + [O II] double-blind study*, *Mon. Not. Roy. Astron. Soc.* **420** (2012) 1926.

[64] M.L.P. Gunawardhana et al., *Galaxy And Mass Assembly: Evolution of the Halpha luminosity function and star formation rate density up to $z < 0.35$*, *Mon. Not. Roy. Astron. Soc.* **433** (2013) 2764 [arXiv:1305.5308] [INSPIRE].

[65] A. Stroe and D. Sobral, *A large narrow band Hα survey at $z \sim 0.2$: the bright end of the luminosity function, cosmic variance and clustering across cosmic time*, *Mon. Not. Roy. Astron. Soc.* **453** (2015) 242 [arXiv:1507.02687].

[66] D. Sobral et al., *CF-HiZELS, an $\sim 10\,deg^2$ emission-line survey with spectroscopic follow-up: Hα [O III] + Hβ and [O II] luminosity functions at $z = 0.8,\ 1.4$ and 2.2*, *Mon. Not. Roy. Astron. Soc.* **451** (2015) 2303 [arXiv:1502.06602] [INSPIRE].

[67] A. Coughlin et al., *Hα Emitting Galaxies at $z \sim 0.6$ in the Deep And Wide Narrow-band Survey*, *Astrophys. J.* **858** (2018) 96.

[68] A.A. Khostovan et al., *A large, deep 3 deg2 survey of Hα, [OIII], and [OII] emitters from LAGER: constraining luminosity functions*, *Mon. Not. Roy. Astron. Soc.* (2020) 171 [arXiv:2001.04989].

[69] S. Harish et al., *A comprehensive study of Hα emitters at $z \sim 0.62$ in the DAWN survey: the need for deep and wide regions*, *Astrophys. J.* **892** (2020) 30 [arXiv:2001.10544].

[70] S. Horiuchi, J.F. Beacom and E. Dwek, *The Diffuse Supernova Neutrino Background is detectable in Super-Kamiokande*, *Phys. Rev. D* **79** (2009) 083013 [arXiv:0812.3157] [INSPIRE].

[71] T. Mauch et al., *The 1.28 GHz MeerKAT DEEP2 Image*, *Astrophys. J.* **888** (2020) 61 [arXiv:1912.06212].

[72] S. Horiuchi, J.F. Beacom, C.S. Kochanek, J.L. Prieto, K.Z. Stanek and T.A. Thompson, *The Cosmic Core-collapse Supernova Rate does not match the Massive-Star Formation Rate*, *Astrophys. J.* **738** (2011) 154 [arXiv:1102.1977] [INSPIRE].

[73] T. Dahlen, L.-G. Strolger, A.G. Riess, S. Mattila, E. Kankare and B. Mobasher, *The Extended Hubble Space Telescope Supernova Survey: The Rate of Core Collapse Supernovae to $z \sim 1$*, *Astrophys. J.* **757** (2012) 70 [arXiv:1208.0342] [INSPIRE].

[74] S. Horiuchi, J.F. Beacom, C.S. Kochanek, J.L. Prieto, K.Z. Stanek and T.A. Thompson, *The Cosmic Core-collapse Supernova Rate does not match the Massive-Star Formation Rate*, *Astrophys. J.* **738** (2011) 154 [arXiv:1102.1977] [INSPIRE].

[75] A. Lien, B.D. Fields and J.F. Beacom, *Synoptic Sky Surveys and the Diffuse Supernova Neutrino Background: Removing Astrophysical Uncertainties and Revealing Invisible Supernovae*, *Phys. Rev. D* **81** (2010) 083001 [arXiv:1001.3678] [INSPIRE].

[76] SUPER-KAMIOKANDE collaboration, *Supernova Relic Neutrino Search at Super-Kamiokande*, *Phys. Rev. D* **85** (2012) 052007 [arXiv:1111.5031] [INSPIRE].

[77] HYPER-KAMIOKANDE collaboration, *Hyper-Kamiokande Design Report*, arXiv:1805.04163 [INSPIRE].

[78] S. Horiuchi, J.F. Beacom and E. Dwek, *The Diffuse Supernova Neutrino Background is detectable in Super-Kamiokande*, *Phys. Rev. D* **79** (2009) 083013 [arXiv:0812.3157] [INSPIRE].

[79] H. Sekiya, *The Super Kamionade Gadolinium Project*, *J. Phys. Conf. Ser.* **1342** (2020) 012044 [INSPIRE].

[80] J.F. Beacom, *The Diffuse Supernova Neutrino Background*, *Ann. Rev. Nucl. Part. Sci.* **60** (2010) 439 [arXiv:1004.3311] [INSPIRE].

[81] KAMIOKANDE-II collaboration, *Observation of a Neutrino Burst from the Supernova SN 1987a*, *Phys. Rev. Lett.* **58** (1987) 1490 [INSPIRE].

[82] K.S. Hirata et al., *Observation in the Kamiokande-II Detector of the Neutrino Burst from Supernova SN 1987a*, *Phys. Rev. D* **38** (1988) 448 [INSPIRE].

[83] R.M. Bionta et al., *Observation of a Neutrino Burst in Coincidence with Supernova SN 1987a in the Large Magellanic Cloud*, *Phys. Rev. Lett.* **58** (1987) 1494 [INSPIRE].

[84] IMB collaboration, *Angular Distribution of Events From Sn1987a*, *Phys. Rev. D* **37** (1988) 3361 [INSPIRE].

[85] E.N. Alekseev, L.N. Alekseeva, V.I. Volchenko and I.V. Krivosheina, *Possible Detection of a Neutrino Signal on 23 February 1987 at the Baksan Underground Scintillation Telescope of the Institute of Nuclear Research*, *JETP Lett.* **45** (1987) 589 [INSPIRE].

[86] SUPER-KAMIOKANDE collaboration, *Search for Supernova Neutrino Bursts at Super-Kamiokande*, *Astrophys. J.* **669** (2007) 519 [arXiv:0706.2283] [INSPIRE].

[87] DUNE collaboration, *Supernova Burst Observations with DUNE*, in *Prospects in Neutrino Physics*, London U.K. (2018), pg. 164 [arXiv:1804.01877] [INSPIRE].

[88] G.A. Tammann, W. Loeffler and A. Schroder, *The Galactic supernova rate*, *Astrophys. J. Suppl.* **92** (1994) 487 [INSPIRE].

[89] S. Ando, J.F. Beacom and H. Yuksel, *Detection of neutrinos from supernovae in nearby galaxies*, *Phys. Rev. Lett.* **95** (2005) 171101 [astro-ph/0503321] [INSPIRE].

[90] K. Nakamura, *Hyper-Kamiokande — a next generation water cherenkov detector*, *Int. J Mod. Phys. A* **18** (2003) 4053.

[91] C.K. Jung, *Feasibility of a next generation underground water Cherenkov detector: UNO*, *AIP Conf. Proc.* **533** (2000) 29 [hep-ex/0005046] [INSPIRE].

[92] A. de Bellefon et al., *MEMPHYS: A Large scale water Cerenkov detector at Frejus*, hep-ex/0607026 [INSPIRE].

[93] MEMPHYS collaboration, *Study of the performance of a large scale water-Cherenkov detector (MEMPHYS)*, *JCAP* **01** (2013) 024 [arXiv:1206.6665] [INSPIRE].

[94] L. Pattavina, N. Ferreiro Iachellini and I. Tamborra, *Neutrino observatory based on archaeological lead*, *Phys. Rev. D* **102** (2020) 063001 [arXiv:2004.06936] [INSPIRE].

[95] TITAND WORKING GROUP collaboration, *Multimegaton water Cherenkov detector for a proton decay search: TITAND (former name TITANIC)*, in *11th International School on Particles and Cosmology*, Karbardino-Balkaria Russia (2001), pg. 288 [hep-ex/0110005] [INSPIRE].

[96] S. Böser, M. Kowalski, L. Schulte, N.L. Strotjohann and M. Voge, *Detecting extra-galactic supernova neutrinos in the Antarctic ice*, *Astropart. Phys.* **62** (2015) 54 [arXiv:1304.2553] [INSPIRE].

[97] M.D. Kistler, H. Yuksel, S. Ando, J.F. Beacom and Y. Suzuki, *Core-Collapse Astrophysics with a Five-Megaton Neutrino Detector*, *Phys. Rev. D* **83** (2011) 123008 [arXiv:0810.1959] [INSPIRE].

[98] H. Yuksel, S. Ando and J.F. Beacom, *Direct measurement of supernova neutrino emission parameters with a gadolinium-enhanced Super-Kamiokande detector*, *Phys. Rev. C* **74** (2006) 015803 [astro-ph/0509297] [INSPIRE].

[99] C. Lunardini and I. Tamborra, *Diffuse supernova neutrinos: oscillation effects, stellar cooling and progenitor mass dependence*, *JCAP* **07** (2012) 012 [arXiv:1205.6292] [INSPIRE].

[100] S.M. Adams, C.S. Kochanek, J.F. Beacom, M.R. Vagins and K.Z. Stanek, *Observing the Next Galactic Supernova*, *Astrophys. J.* **778** (2013) 164 [arXiv:1306.0559] [INSPIRE].

[101] A. Nikrant, R. Laha and S. Horiuchi, *Robust measurement of supernova ν_e spectra with future neutrino detectors*, *Phys. Rev. D* **97** (2018) 023019 [arXiv:1711.00008] [INSPIRE].

[102] S. Horiuchi and J.P. Kneller, *What can be learned from a future supernova neutrino detection?*, *J. Phys. G* **45** (2018) 043002 [arXiv:1709.01515] [INSPIRE].

[103] J. Migenda, *Supernova Model Discrimination with Hyper-Kamiokande*, Ph.D. Thesis, Sheffield University, Sheffield U.K. (2019). arXiv:2002.01649 [INSPIRE].

[104] M.T. Keil, G.G. Raffelt and H.-T. Janka, *Monte Carlo study of supernova neutrino spectra formation*, *Astrophys. J.* **590** (2003) 971 [astro-ph/0208035] [INSPIRE].

[105] I. Tamborra, B. Müller, L. Hudepohl, H.-T. Janka and G. Raffelt, *High-resolution supernova neutrino spectra represented by a simple fit*, *Phys. Rev. D* **86** (2012) 125031 [arXiv:1211.3920] [INSPIRE].

[106] T. Yoshida, T. Kajino and D.H. Hartmann, *Constraining the spectrum of supernova neutrinos from neutrino-process-induced light-element synthesis*, *Phys. Rev. Lett.* **94** (2005) 231101 [astro-ph/0505043] [INSPIRE].

[107] C. Lunardini, *Diffuse neutrino flux from failed supernovae*, *Phys. Rev. Lett.* **102** (2009) 231101 [arXiv:0901.0568] [INSPIRE].

[108] I. Tamborra, *Supernova Neutrinos: Theory*, in *Prospects in Neutrino Physics*, London U.K. (2015) [arXiv:1604.07332] [INSPIRE].

[109] A. Priya and C. Lunardini, *Diffuse neutrinos from luminous and dark supernovae: prospects for upcoming detectors at the $O(10)$ kt scale*, *JCAP* **11** (2017) 031 [arXiv:1705.02122] [INSPIRE].

[110] T. Totani, K. Sato, H.E. Dalhed and J.R. Wilson, *Future detection of supernova neutrino burst and explosion mechanism*, *Astrophys. J.* **496** (1998) 216 [astro-ph/9710203] [INSPIRE].

[111] K. Nakazato, K. Sumiyoshi, H. Suzuki, T. Totani, H. Umeda and S. Yamada, *Supernova Neutrino Light Curves and Spectra for Various Progenitor Stars: From Core Collapse to Proto-neutron Star Cooling*, *Astrophys. J. Suppl.* **205** (2013) 2 [arXiv:1210.6841] [INSPIRE].

[112] I. Tamborra, G. Raffelt, F. Hanke, H.-T. Janka and B. Mueller, *Neutrino emission characteristics and detection opportunities based on three-dimensional supernova simulations*, *Phys. Rev. D* **90** (2014) 045032 [arXiv:1406.0006] [INSPIRE].

[113] D. Vartanyan, A. Burrows, D. Radice, A.M. Skinner and J. Dolence, *A Successful 3D Core-Collapse Supernova Explosion Model*, *Mon. Not. Roy. Astron. Soc.* **482** (2019) 351 [arXiv:1809.05106] [INSPIRE].

[114] S.M. Couch, M.L. Warren and E.P. O'Connor, *Simulating Turbulence-aided Neutrino-driven Core-collapse Supernova Explosions in One Dimension*, arXiv:1902.01340 [INSPIRE].

[115] HYPER-KAMIOKANDE collaboration, *Physics potentials with the second Hyper-Kamiokande detector in Korea*, *PTEP* **2018** (2018) 063C01 [arXiv:1611.06118] [INSPIRE].

[116] C. Lunardini, *Diffuse supernova neutrinos at underground laboratories*, *Astropart. Phys.* **79** (2016) 49 [arXiv:1007.3252] [INSPIRE].

[117] J.F. Beacom and M.R. Vagins, *GADZOOKS! Anti-neutrino spectroscopy with large water Cherenkov detectors*, *Phys. Rev. Lett.* **93** (2004) 171101 [hep-ph/0309300] [INSPIRE].

[118] K.R. Bays, *Search for the Diffuse Supernova Neutrino Background at Super-Kamiokande*, Ph.D. Thesis, University of California Irvine, Irvine U.S.A. (2012).

[119] T. Garn and P.N. Best, *Predicting dust extinction from the stellar mass of a galaxy*, *Mon. Not. Roy. Astron. Soc.* **409** (2010) 421.

[120] R.C. Kennicutt, Jr., *The Integrated spectra of nearby galaxies: General properties and emission line spectra*, *Astrophys. J.* **388** (1992) 310 [INSPIRE].

[121] R.C. Kennicutt, Jr., *Star formation in galaxies along the Hubble sequence*, *Ann. Rev. Astron. Astrophys.* **36** (1998) 189 [astro-ph/9807187] [INSPIRE].

[122] P. Schechter, *An analytic expression for the luminosity function for galaxies*, *Astrophys. J.* **203** (1976) 297 [INSPIRE].

[123] W. Saunders et al., *The 60-micron and far-infrared luminosity functions of IRAS galaxies*, *Mon. Not. Roy. Astron. Soc.* **242** (1990) 318 [INSPIRE].

[124] G. Chabrier, *Galactic stellar and substellar initial mass function*, *Publ. Astron. Soc. Pac.* **115** (2003) 763 [astro-ph/0304382] [INSPIRE].

[125] I.K. Baldry and K. Glazebrook, *Constraints on a universal IMF from UV to near-IR galaxy luminosity densities*, *Astrophys. J.* **593** (2003) 258 [astro-ph/0304423] [INSPIRE].

[126] P. Kroupa, *On the variation of the initial mass function*, *Mon. Not. Roy. Astron. Soc.* **322** (2001) 231.

[127] J.M. Scalo, *The Stellar initial mass function*, *Fund. Cosmic Phys.* **11** (1986) 1.

[128] A.M. Hopkins, A.J. Connolly, D.B. Haarsma and L.E. Cram, *Towards a resolution of the discrepancy between different estimators of star formation rate*, *Astron. J.* **122** (2001) 288 [astro-ph/0103253] [INSPIRE].

[129] SDSS collaboration, *Star formation rate indicators in the Sloan Digital Sky Survey*, *Astrophys. J.* **599** (2003) 971 [astro-ph/0306621] [INSPIRE].

[130] M.A.W. Verheijen, *The Ursa Major Cluster of Galaxies. 5. H I Rotation Curve Shapes and the Tully-Fisher Relations*, *Astrophys. J.* **563** (2001) 694 [astro-ph/0108225] [INSPIRE].

[131] J.F. Helmboldt, R.A.M. Walterbos, G.D. Bothun, K. O'Neil and W.J.G. de Blok, *Star formation in HI selected galaxies 1: Sample characteristics*, *Astrophys. J.* **613** (2004) 914 [astro-ph/0406317] [INSPIRE].

[132] S.J. Smartt, *Observational constraints on the progenitors of core-collapse supernovae: the case for missing high mass stars*, *Publ. Astron. Soc. Austral.* **32** (2015) e016 [arXiv:1504.02635] [INSPIRE].

[133] W. Zhang et al., *Experimental Limit on the Flux of Relic Anti-neutrinos From Past Supernovae*, *Phys. Rev. Lett.* **61** (1988) 385 [INSPIRE].